Path Following Control Design for Passenger Comfort Under Disturbances

Shiyu Wan

Master of Science Thesis

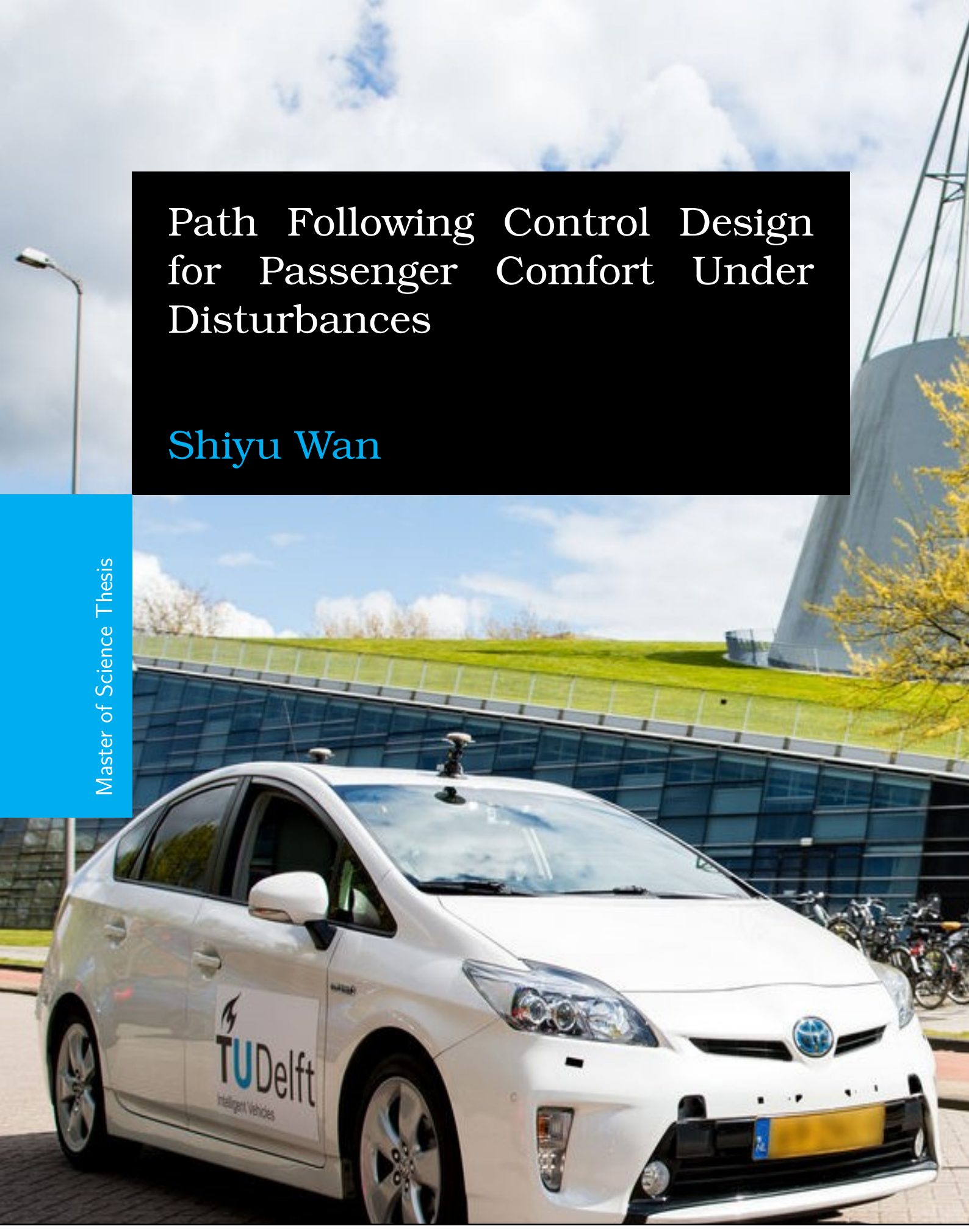

TU Delft Delft University of Technology

Path Following Control Design for Passenger Comfort Under Disturbances

Master of Science Thesis

For the degree of Master of Science in Mechanical Engineering at Delft University of Technology

Shiyu Wan

December 17, 2018

Faculty of Mechanical, Maritime and Materials Engineering (3mE) · Delft University of Technology

Abstract

In recent years, enormous progress has been made in the field of automated driving. As a consequence, automated driving technologies are becoming increasingly popular. Research on comfort for autonomous vehicles, however, is still limited and unexplored. Some researchers address the comfort issue in path planning by velocity profiles, which regulates the instantaneous values of vehicle acceleration and jerk. Meanwhile, the actuator response to external disturbances and the inaccurate following can result in the violation to the pre-designed path, and therefore causes an uncomfortable driving experience. In order to tackle the passenger comfort issue from the perspective of path following control, this study proposes a frequency shaped model predictive control scheme that is (i) robust under external disturbances and (ii) able to optimize passenger comfort by regulating the vehicle lateral acceleration with respect to its corresponding frequency. The frequency is selected based on the comfort evaluation criteria proposed in ISO 2631. Further, the proposed controller is tested in three simulation scenarios, compared to three baseline controllers with respect to tracking accuracy and driving comfort. Finally, our analysis shows that the FSMPC controller can improve driving comfort, especially at the velocity higher than 60 km/h.

Table of Contents

List of Figures

List of Tables

Acknowledgements

I would like to thank my supervisor Dr.ir. Riender Happee for providing the chance to work on this graduation project, and also for his valuable guidance through the work.

I would like to thank my daily supervisor Dr. Laura Ferranti for being an amazing mentor. I am grateful for her help on the project, and on writing the thesis.

I would also thank Dr. Barys Shyrokau and Tugrul Irmak for their advise from the perspectives of vehicle dynamics and human factor.

Last but not least, I would like to express my gratitude to my parents for their support in the past two and a half years.

Delft, University of Technology — Shiyu Wan
December 17, 2018

“我告诉你啊，那个洞的深处一定有黄金的。”

—— 《大裂》

Chapter 1

Introduction

1-1 Background

In recent years, enormous research progress on automated driving has been made. By reducing the human intervention, automated driving has the ability to eliminate human errors and reduce the response time. This leads to the improvement in driving safety and driving efficiency [3]. The development of automated vehicles is becoming much more popular in the recent years. Several automated systems have been used in the automated industry. The advanced driver assistance systems (ADAS) such as lane keeping assistance (LKA) and automated emergency braking (AEB) are popular among the car manufacturers. There are also some examples of the automated driving system implementation above level 3 (L3): Tesla L3 autopilot system has been embedded in their Model S and Model X vehicles [4], Google self-driving car project Waymo drove for more than five million miles across the US [5].

As the technology of automated system becomes more and more mature in recent years, the research focus tends to turn to the investigation on user acceptance to ADAS, as well as how to improve the acceptance. It was found that most people were positive towards automated driving, while the majority of their concern was about the safety and legal issues [6]. Meanwhile, comfort as another key factor, its study on automated vehicle is still a novel topic [7]. Although the subjective study of automated driving comfort is extremely limited, there are some user surveys indicating that passengers would connect comfort to acceleration [8, 9]. Further, in the automated driving comfort study on simulator of Yusof et al. [10], the comfort is linked to driving style, which is categorized by acceleration magnitude. It is therefore reasonable to improve driving comfort by manipulating the vehicle acceleration.

To provide an automated driving experience as comfortable as manual driving has draw the attentions of researchers, whose studies are mainly focused on the longitudinal direction and solved by path planning design. The common solution is to implement the velocity profiles that constrain the vehicle acceleration and jerk [11, 12], based on the comfort thresholds of acceleration and jerk [2, 13]. Although the investigation of passenger comfort on automated vehicles at the lateral direction is not that popular, related studies can be found in the

design of path planning by Svensson and Eriksson [14], where the importance of acceleration frequency was addressed.

From the perspective of passenger perception, the discomfort comes from the perceived vehicle vibration, which is due to the vehicle motion, especially when the vehicle is subjected to some external disturbances. Unlike the human driver that can change their driving behavior according to the actual situation, the automated system might exert an intensive control input to guarantee tracking accuracy at the cost of discomfort. Hence, apart from the smooth trajectory generated by the path planning algorithm, the driving comfort can be further improved in the path following with a smooth response to the reference path especially at the presence of disturbances, which also requires the controller to be robust.

1-2 Passenger comfort in path following

The literature shows that most of the popular control methods are robust against disturbance, such as fuzzy logic control (FLC) [15, 16], sliding mode control (SMC) [17, 18] and model predictive control (MPC) [19–21]. However, it is noted that only few of those studies took driving comfort into consideration. Driving comfort due to motion vibration is evaluated by the acceleration magnitude coordinated with its corresponding frequency. Furthermore, the bicycle model, as a widely-adopted vehicle model in path following control design, does not include lateral acceleration in its state variables. Therefore the optimization of lateral acceleration is rarely included in the controller design. On the other hand, the motion comfort is already considered in the motion planner by bounding the overall acceleration below a certain value [12, 22], it may let the researchers regard the comfort optimization in path following as unnecessary. Yet, high lateral acceleration can still be found, especially when the disturbances are applied [23]. Hence, comfort optimization in path following control design is desired and necessary.

Among those studies that considered driving comfort, one way is to control the instantaneous acceleration under a certain value [24, 25]. Apart from implementing acceleration constraints, Lima et al. [26] proposed a clothoid-based MPC that made a trade-offs between the tracking accuracy and path smoothness, where the low jerk and smooth curve were generated. Besides, a comfort controller added to the path following controller was proposed by Whitsitt and Sprinkle [27]. The authors conducted the system identification between velocity and steering angle of human drivers to produce a comfort range, based on which the comfort controller was used to keep the steering rate and velocity below the fitting curve.

However, although the methods mentioned above can enhance the comfort performance to some extent, according to ISO 2631, another important factor of comfort evaluation is missing, that is, the frequency spectrum of the acceleration. The passenger can still feel uncomfortable if the acceleration is at a sensitive frequency, even though the acceleration is bounded by a reasonably low value. Further, such hard constraints can affect the vehicle handling performance and even cause safety problems under emergency situations where the large acceleration is unavoidable (i.e. double lane change). Therefore, it is important for the path following controller design to take both the acceleration and frequency into account, while being able to make a trade-off between comfort and tracking performance. A path following controller using frequency shaped linear quadratic (FSLQ) algorithm was developed by Peng

and Tomizuka [28], where the cost function was shaped into frequency domain, so that the weighting factors in cost function could be frequency dependent. Hence, the acceleration could be optimized with respect to both magnitude and frequency, whilst the steer input was regulated regarding both tracking accuracy and driving comfort.

1-3 Proposed solution and objectives

This study aims at designing a path following controller with comfort optimization. As the path following controller usually refers to the control of steering system that influences the vehicle lateral motion, this study focuses on the comfort optimization on the lateral direction. We rely on the frequency shaped cost function in FSLQ controller [28], taking the advantage of frequency optimization as well as comfort-tracking balancing. Further, since control input constraints are desired, a linear model predictive controller with frequency shape cost function is developed. In this study, a frequency shaped model predictive controller (FSMPC) will be used to control a nonlinear 9 degree-of-freedom (DOF) vehicle plant to follow the signals from path planning module (Figure 1-1). The proposed solution is detailed in Chapter 4. The related methodology study on FSMPC algorithm can be found in [29, 30].

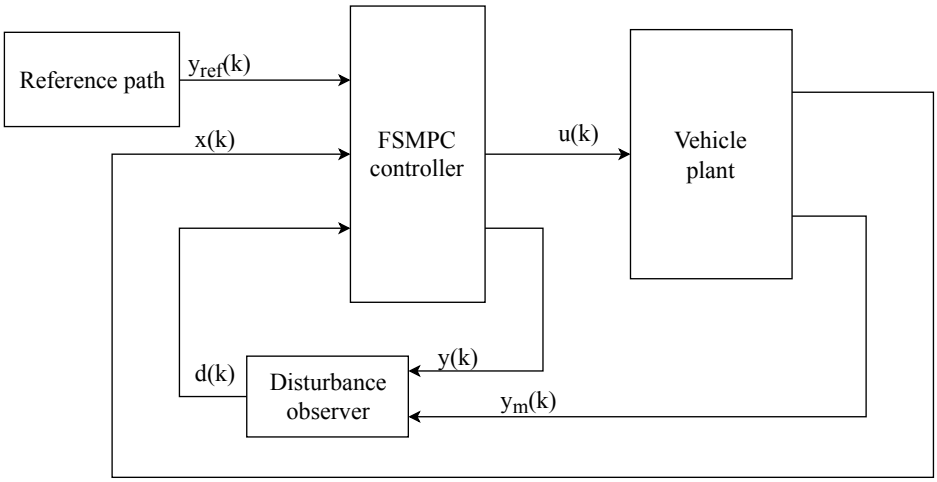

Figure 1-1: Proposed FSMPC control scheme.

In order to develop and evaluate the performance of the proposed FSMPC controller, the thesis focuses on the following problems

- Find the ride comfort evaluation methods that can be adopted for path-following control design.
- Develop a baseline controller that does not specifically consider driving comfort as the benchmark.
- Develop a FSMPC controller that is able to balance the driving comfort with tracking performance.
- Evaluate the controller performance on driving comfort based on the simulation result, where the simulation scenarios emphasize disturbance rejection and passenger comfort.

1-4 Outline

The evaluation criteria for driving comfort is summarized in Chapter 2. The vehicle model used in the controller design and the disturbance models for simulation are summarized in Chapter 3. The controller design algorithm is described in detail in Chapter 4. The experiment scenarios and the experimental results are presented in Chapter 5, where the performance of baseline controllers and FSMPC controller are compared. Lastly, the conclusion and future works are summarized in Chapter 6.

Chapter 2

Driving comfort evaluation

Taking the concept of improving comfort by the absence of discomfort [31], the feasible driving comfort assessment criteria will be implemented in the controller design. This chapter summarizes the comfort evaluation methods that are applicable for such implementation. Firstly, we describe the International Standard ISO 2631 as comfort quantification widely applied to vehicle comfort design. Secondly, we describe the influence of instant acceleration values on driving comfort. Finally, we describe the comfort study in the frequency domain.

As this study targets the discomfort mitigation on the lateral direction by steering motion control, the summary of driving comfort evaluation will only focus on the lateral direction.

2-1 The ISO 2631 standard

ISO 2631 quantifies the human exposure to vibration using the index of frequency weighted root-mean-square (r.m.s) acceleration for three transitional directions (x, y, z) and three rotational directions (row, pitch, yaw). The index is connected to general discomfort (0.5 - 80 Hz) and motion sickness (0.1 - 0.5 Hz) by different weighting factors.

For general discomfort in the lateral direction, the basic evaluation is calculated as follows, using the weighting curve W_d given in Figure 2-1.

$$a_{y,\mathrm{wd}} = \left[\frac{1}{T}\int_0^T {a^2}_{y,\mathrm{wd}}(t)dt\right]^{\frac{1}{2}} \tag{2-1}$$

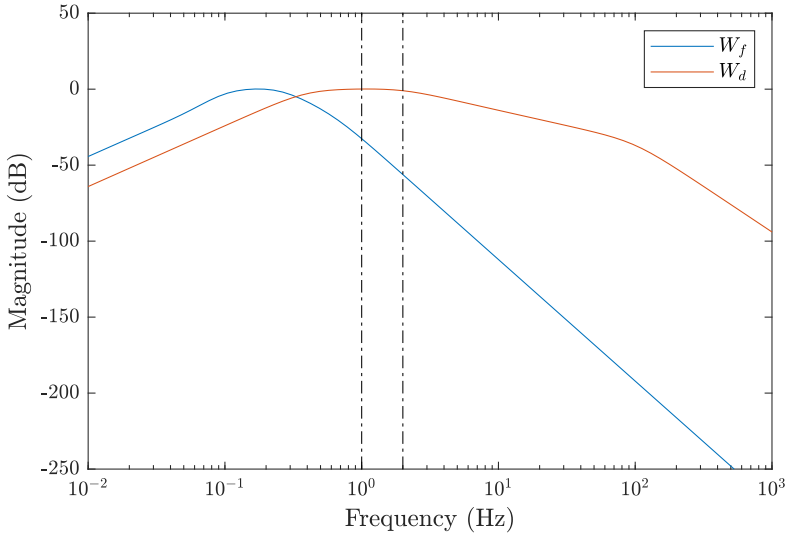

Figure 2-1: Frequency weighting curves (W_d for y direction, W_f for motion sickness). The sensitive frequency range for lateral general discomfort is indicated between the dash-dot lines.

When the vehicle is suffering occasional shocks and transient vibration from external disturbances, crest factor rises. The crest factor is defined as the modulus of the ratio of the maximum instantaneous peak value of the frequency-weighted acceleration signal to its r.m.s value [2]. When the crest factor is higher than 9, the basic evaluation may underestimate the severity of discomfort, which requires the correction by additional evaluation methods.

Running r.m.s method is one of the additional evaluations. It integrates the acceleration in a short time period τ over the measurement period T. Then the evaluation index is given by the maximum transient vibration value (MTVV). Its calculation in the lateral direction for general discomfort is given as follows

$$\begin{aligned} a_{y,\mathrm{wd}}(t_0) &= \left[\frac{1}{\tau}\int_{t_0-\tau}^{t_0} {a^2}_{y,\mathrm{wd}}(t)dt\right]^{\frac{1}{2}} \\ \mathrm{MTVV} &= \max\left[a_{y,\mathrm{wd}}(t_0)\right] \end{aligned} \tag{2-2}$$

The magnitude of $a_{y,\mathrm{wd}}$ is related to the comfort level over the measured time period, where the smaller value represents less discomfort incidence (Table 2-1).

Table 2-1: Comfort reaction to vibration [2].

Less than 0.315 m/s^2	not uncomfortable
0.315 m/s^2 to 0.63 m/s^2	a little uncomfortable
0.5 m/s^2 to 1 m/s^2	fairly uncomfortable
0.8 m/s^2 to 1.6 m/s^2	uncomfortable
1.25 m/s^2 to 2.5 m/s^2	very uncomfortable
Greater than 2 m/s^2	extremely uncomfortable

Similar to the general discomfort in the lateral direction, motion sickness can be evaluated by the value r.m.s acceleration weighted by W_f, where the frequency weighting function W_f in Figure 2-1 is only applicable for vertical direction. Also, the incidence of motion sickness is evaluated by the motion sickness dose value (MSDV) using the acceleration knowledge throughout the whole vibration period. The higher value of MSDV indicates the higher likelihood of motion sickness.

In order to calculate the motion sickness indices for lateral direction ($a_{y,ms}$ and MSDV$_y$), we use another weighting function that is further introduced in section 2-3. Then the calculation of $a_{y,ms}$ and MSDV$_y$ are written as follows.

$$a_{y,\mathrm{ms}} = \left[\frac{1}{T}\int_0^T {a^2}_{y,\mathrm{ms}}(t)dt\right]^{\frac{1}{2}} \tag{2-3}$$

$$\mathrm{MSDV}_y = \left[\int_0^T {a^2}_{y,\mathrm{ms}}(t)dt\right]^{\frac{1}{2}} \tag{2-4}$$

2-2 Comfort and acceleration

Apart from r.m.s acceleration, the peak value of acceleration is also considered as an important index for ride comfort assessment, for the purpose of improving the performance under extreme vibration that requires maintenance attentions [32].

The study of Cheng [33] scaled the lateral acceleration into three endurance levels:

- 1.8 m/s^2 for comfort,
- 3.6 m/s^2 for medium comfort,
- 5 m/s^2 for discomfort.

The experimental study on highway by Xu et al. [34] found that drivers would like to control the lateral acceleration lower than 1.8 m/s^2. Yamagishi et al. [35] studied the relationship between discomfort and lateral acceleration during cornering, which indicated that the subjects feel comfort with the lateral acceleration lower than 1.75 m/s^2 with resting posture (most of the ratings are below 1), while they tended to be more sensitive to lateral acceleration with reading and lying postures. In addition, the lateral acceleration study of Kilinç and Baybura [36] adopted 1.47 m/s^2 as the threshold.

Under the external disturbances, passengers in vehicle may feel shocks that come from the sudden change of acceleration, in another word, jerk. Some studies showed that jerk is also important to passenger comfort [37, 38], and it is taken into consideration in some path planning designs [39, 40]. However jerk is usually not taken into account for path following, due to the limitation of model size and computational time.

2-3 Comfort evaluation in frequency domain

In order to filter the vibration frequencies that lead to higher level of discomfort with the propose controller, we need to understand how the vibration frequency in lateral direction affects the passenger comfort.

In the interested frequency range of general discomfort, the most discomfort was found at the frequency of 2 Hz on the lateral oscillation, in the experiment range of 1 Hz to 30 Hz [41]. It was found by Beard and Griffin [42] that the sensitivity of human comfort to the lateral vibration increases as the increasing of the acceleration frequency in the range of 0.2-1.0 Hz, which is similar to the result found in the study of Wyllie and Griffin [43], in the frequency range of 0.2-1.6 Hz with backrest. Further, it was found that the lateral acceleration with the frequencies between 1.25 and 2.0 Hz causes the most discomfort, in the experiment range of 0.5-5.0 Hz [44]. These studies are consistent with the description of frequency weighting function W_d.

As for motion sickness, Donohew and Griffin [1] pointed out that the horizontal accelerations at frequencies less than 0.2 Hz are significant in road and rail transport. The authors developed a lateral acceleration frequency weighting scheme $W_{f,\text{lateral}}$ for motion sickness as shown in Figure 2-2, based on the subjective illness rating in the frequency range 0.0315-0.2 Hz [1], as well as the motion sickness experiment results obtained from lateral oscillation in the frequency range of 0.2-0.8 Hz [45, 46]. Combining this weighting curve with W_d given in Figure 2-1, the lateral acceleration is able to be optimized regarding both general discomfort ($a_{y,\text{wd}}$) and motion sickness ($a_{y,\text{ms}}$).

2-4 Summary

ISO 2631-1 evaluates driving comfort on the acceleration magnitude, its corresponding frequency, and the time of exposure. For the passenger comfort evaluation, it is more precise than only focusing on the instantaneous value of acceleration. It is therefore a more proper choice to implement the calculation of $a_{y,\text{wd}}$ and $a_{y,\text{ms}}$ in the controller design for comfort optimization, rather than simply adding constraints on the lateral acceleration. Hence, the controller is required to optimize the acceleration while filtering the undesired frequencies. The frequency weighting curve W_d shall be adopted for general discomfort, whilst the frequency weighting curve $W_{f,\text{lateral}}$ shall be adopted for motion sickness.

As for the controller performance evaluation, the value of $a_{y,\text{ms}}$ and $a_{y,\text{wd}}$ shall be used to estimate the overall comfort, while the peak value of acceleration can be used to evaluate the local comfort.

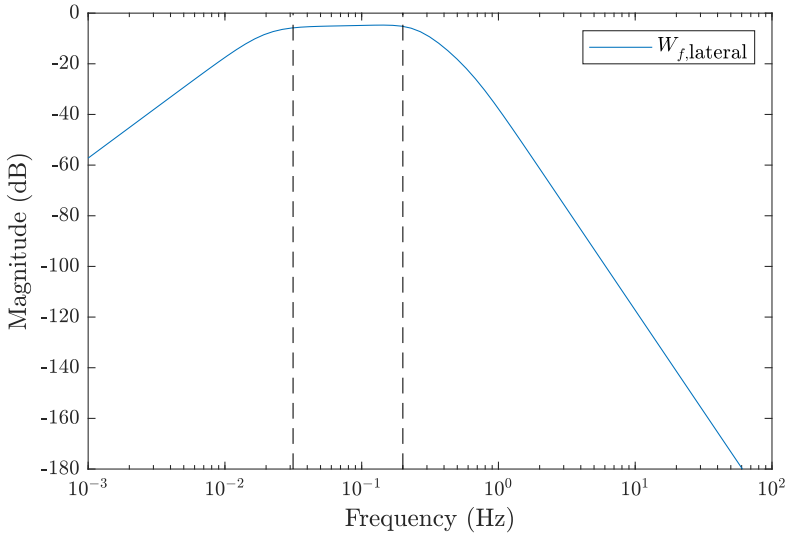

Figure 2-2: Realizable frequency weighting curve for lateral acceleration, derived from the normalized mild nausea incidence by Donohew and Griffin [1]. The sensitive frequency range for lateral motion sickness is indicated between the dash lines.

Chapter 3

Modelling

This chapter introduces the models used in simulation. The MPC controller uses a two-track linear dynamics bicycle model translated to the global frame as the prediction model. Three external disturbances that typically affect both tracking accuracy and passenger comfort are modelled in the simulation: crosswind, friction change, and sensor noise.

3-1 Vehicle modelling

3-1-1 Tire model

Given that the tires are the only components in contact with the road surface, the modelling of tire behaviour is very important. Due to the high nonlinearity of the tire behaviour, several models have been developed using different approaches, such as Magic Formula, Dugoff model and brush model. The Magic Formula is the most well-accepted model among them. This model is developed using the empirical approach, which requires a big amount of full scale tire tests to explore formula coefficients to reconstruct the tire force.

The complexity of the nonlinear tire model would increase the computational burden of the controller. Therefore a linear tire model is frequently used in vehicle modelling. The linear model linearized the nonlinear tire model until the slip increases to a certain value, while most of the daily driving condition lays in the linear range.

For the lateral direction, such a linear relationship is found between the slip angle and lateral force as given in the follows. The linear coefficient called cornering stiffness is dependent on the tire nature, which is possible to be derived from Magic Formula. The lateral forces for front and rear tires are calculated separately as follows

$$\begin{aligned} F_{y,f} &= C_{\alpha f}\alpha_f \\ F_{y,r} &= C_{\alpha r}\alpha_r \end{aligned} \tag{3-1}$$

$$\begin{aligned} \alpha_f &= \delta - \frac{v + l_f r}{u} \\ \alpha_r &= -\frac{v - l_r r}{u} \end{aligned} \tag{3-2}$$

$$C_\alpha = P_{\mathrm{KY1}} F_{z0} \sin\left[P_{\mathrm{KY4}} \arctan\left(\frac{F_z}{P_{\mathrm{KY2}} F_{z0}}\right)\right] \tag{3-3}$$

where F_y denotes the lateral force on front tires, C_α denotes the cornering stiffness, α denotes the slip angle, δ denotes the steering angle, v denotes the lateral velocity, u denotes the forward speed, r denotes the yaw rate, l denotes the distance from axle to center of gravity (COG), F_z denotes the vertical load, and P_{KY} denotes the identification coefficients of Magic Formula. f and r denote the front and rear respectively.

3-1-2 Dynamic bicycle model

As the vehicle lateral control is dominated by the lateral and yaw motion, the 2-DOF bicycle model (Figure 3-1) is adopted.

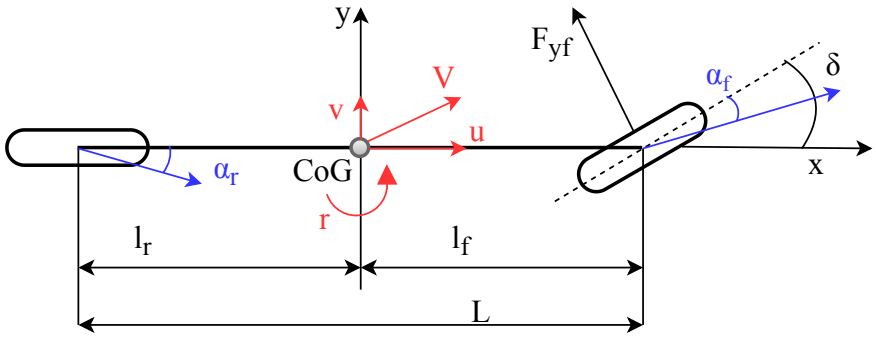

Figure 3-1: Bicycle model.

The bicycle model is a simple form to model the vehicle handling with several assumptions for such simplification. The forward speed is assumed constant, since only the lateral and yaw motion are modelled. The lateral and longitudinal load transfers are ignored, so as the roll, pitch and vertical motion. The bicycle model also limits its modeling range by assuming small steering angle and ignoring the self-aligning moment. The general bicycle model is given as follows.

$$\begin{aligned} ma_y &= m(\dot{v} + ur) = F_{yf} + F_{yr} \\ I_z \dot{r} &= l_f F_{yf} - l_r F_{yr} \end{aligned} \tag{3-4}$$

where m denotes the vehicle mass, a_y denotes the lateral acceleration, $\dot{v}$ denotes the change rate of lateral velocity, $\dot{r}$ denotes the change rate of yaw rate.

Substituting the tire forces in (3-4) with the linear tire model given in (3-1) and (3-2), the linear dynamic bicycle model adopted in MPC prediction model is written as follows

$$\begin{bmatrix} \dot{v} \\ \dot{r} \end{bmatrix} = \begin{bmatrix} -\frac{C_{\alpha f}+C_{\alpha r}}{mu} & -u+\frac{l_r C_{\alpha r}-l_f C_{\alpha f}}{mu} \\ \frac{l_r C_{\alpha r}-l_f C_{\alpha f}}{I_z u} & -\frac{{l_r}^2 C_{\alpha r}+{l_f}^2 C_{\alpha f}}{I_z u} \end{bmatrix} \begin{bmatrix} v \\ r \end{bmatrix} + \begin{bmatrix} \frac{C_{\alpha f}}{m} \\ \frac{l_f C_{\alpha f}}{I_z} \end{bmatrix} \delta \tag{3-5}$$

Noted that due to the limitation of linear tire model, the linear bicycle model does not have good approximation to the real vehicle plant if the slip angle is larger than ± 5 deg.

For the purpose of comfort optimization, the lateral acceleration a_y is supposed to be taken in to account in the vehicle modelling as given in (3-6).

$$a_y = \begin{bmatrix} -\frac{C_{\alpha f}+C_{\alpha r}}{mu} & \frac{l_r C_{\alpha r}-l_f C_{\alpha f}}{mu} \end{bmatrix} \begin{bmatrix} v \\ r \end{bmatrix} + \frac{C_{\alpha f}}{m} \delta \tag{3-6}$$

3-1-3 Modelling in the absolute inertia frame

Since the vehicle states and output signals given by the linear bicycle model lays in the local frame, the motion equations need to be translated to the inertia frame by the follow equations

$$\begin{aligned} \dot{Y} &= u \sin\psi + v \cos\psi \\ \dot{X} &= u \cos\psi - v \sin\psi \end{aligned} \tag{3-7}$$

where $\dot{Y}$ denotes the change rate of lateral position Y in the global frame, $\dot{X}$ denotes the change rate of longitudinal position in the global frame, ψ denotes the yaw angle.

As a linear MPC controller will be eventually developed, (3-7) is linearized with small yaw angle assumption as follows

$$\begin{aligned} \dot{Y} &= u\psi + v \\ \dot{X} &= u - v\psi \end{aligned} \tag{3-8}$$

3-1-4 Summary

The MPC prediction model involves the concept of vehicle state, system output, and control input. The vehicle state is a set of variables that describes the current vehicle behaviour. As we focus on the path following in the lateral direction, the lateral velocity, yaw rate, lateral position as well as yaw angle are involved, $x = [\ v \quad r \quad Y \quad \psi\ ]^T$. Accordingly, the system output is supposed to be the utilized tracking signals: lateral position and yaw angle of the vehicle, $y = [\ Y \quad \psi\ ]^T$. As we only consider the two wheel steering (2WS) system in this study, the control input will be the front steering angle, $u = \delta$.

With the vehicle model described in (3-5) and (3-8), the prediction model in continuous-time state space is written as follows.

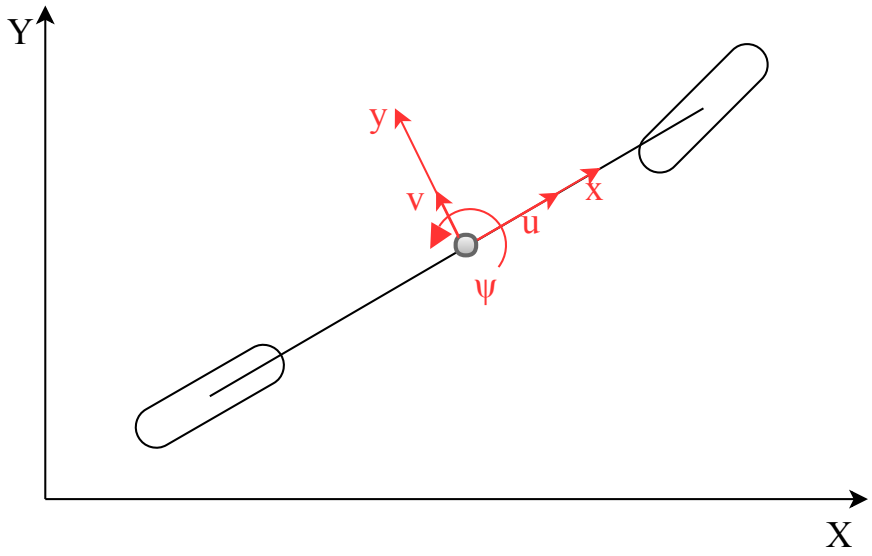

Figure 3-2: Vehicle model in absolute inertia frame.

Vehicle state:

$$\underbrace{\begin{bmatrix} \dot{v} \\ \dot{r} \\ \dot{Y} \\ \dot{\psi} \end{bmatrix}}_{\dot{x}} = \underbrace{\begin{bmatrix} -\frac{C_{\alpha f}+C_{\alpha r}}{mu} & -u+\frac{l_r C_{\alpha r}-l_f C_{\alpha f}}{mu} & 0 & 0 \\ \frac{l_r C_{\alpha r}-l_f C_{\alpha f}}{I_z u} & -\frac{{l_r}^2 C_{\alpha r}+{l_f}^2 C_{\alpha f}}{I_z u} & 0 & 0 \\ 1 & 0 & 0 & u \\ 0 & 1 & 0 & 0 \end{bmatrix}}_{A} \underbrace{\begin{bmatrix} v \\ r \\ Y \\ \psi \end{bmatrix}}_{x} + \underbrace{\begin{bmatrix} \frac{C_{\alpha f}}{m} \\ \frac{l_f C_{\alpha f}}{I_z} \\ 0 \\ 0 \end{bmatrix}}_{B} \delta \tag{3-9}$$

System output:

$$\underbrace{\begin{bmatrix} Y \\ \psi \end{bmatrix}}_{y} = \underbrace{\begin{bmatrix} 0 & 0 & 1 & 0 \\ 0 & 0 & 0 & 1 \end{bmatrix}}_{C} \begin{bmatrix} v \\ r \\ Y \\ \psi \end{bmatrix} \tag{3-10}$$

In order to be used in the MPC controller, the continuous-time state space summarized above should be discretized regarding the sampling time T_s.

3-2 Disturbance modelling

3-2-1 Crosswind

The crosswind effect is one of the common external disturbances that cause unwanted lateral motion and affect the vehicle stability. As indicated in Figure 3-3, as the consequences of the

disturbance force F_w and torque M_w exerted by crosswind, the velocity composition between wind velocity v_w and vehicle velocity v_x forces the vehicle to deviate from the original path. Such deviation accumulates over time even after the crosswind stops. Besides, since both of lateral acceleration and yaw rate have fast response to crosswind, passengers can feel uncomfortable if they perceive the transient vibration.

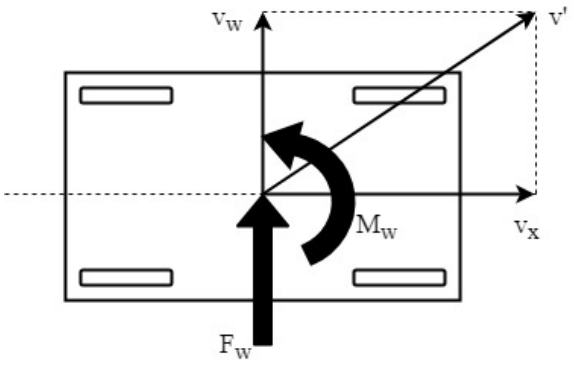

Figure 3-3: Disturbance force and vehicle velocity with crosswind.

In the simulations of automated driving system, Yakub et al. [47] used sine wave to model the small typhoon, whilst Fuller et al. [48] adopted the Dryden filter to represent the natural occurring windy condition. However, for path following, the crosswind is usually modeled by a lateral step input at a 90 degrees angle to the vehicle with the velocity of 10 m/s [19, 20, 28], as it produces the extreme windy condition for vehicle lateral control. Further, the numerical study by William et al. [49] indicated that the wind gust velocity higher than 10 m/s has a critical influence the vehicle lateral response. It is also indicated by Abe [50] that magnitudes of wind gust between 10 and 25 m/s have the major impact on vehicle handling.

In the simulation of this study, the crosswind will be model as a step input of 10 m/s, represented by the side force F_w and side moment M_w acting on the vehicle plant. Their magnitudes are approximated by (3-11), which is also used in the other path following studies [20, 21].

$$\begin{aligned} F_w &= \frac{2.5\pi}{2} {v_w}^2 \\ M_w &= (2.5\frac{\pi}{2} - 3.3(\frac{\pi}{3})^3){v_w}^2 + \frac{l_f - l_r}{2} F_w \end{aligned} \tag{3-11}$$

3-2-2 Friction changes

The sudden drop of road friction during aggressive cornering decreases the lateral force rapidly, and therefore changes the lateral acceleration in a short time. It can be regarded as a step or impulse force input to the vehicle in the lateral direction, depending on the actual time when the vehicle is driving on the low friction surface. In either case, the vehicle will response with the side slip motion to such a force change [50], causing discomfort and vehicle instability. To endure the friction drops on the road surface is a basic requirement for the robust design of path following controller, where the icy road ($\mu = 0.1$) and wet asphalt ($\mu = 0.5$) are typically studied for low friction surface [18, 19].

In order to test the controller by its disturbance rejection ability as well as its performance on low friction surface, the friction change is modelled as step input from dry asphalt ($\mu = 1$) to icy surface ($\mu = 0.1$).

3-2-3 Sensor noise

Because the sensor detection is not always accurate, the situation of wrongly calculating the distance and being corrected after a while always happens. Such error affects the self-localization of the vehicle, especially when the localization is dependent on the distance between vehicle and the surroundings by sensor fusion of radar, lidar and IMU rather than the GPS, where the localization is very sensitive to the change of environment. Due to the range of the sensors, such kind of error can increase further when the vehicle enters an intersection [51]. Such sensor noise leads to the vibration of vehicle localization. In order to correct the perceived localization error, the frequent change of lateral acceleration that causes discomfort is excited by the steer input.

In our simulation, such sensor noise on lateral positioning is modelled as white noise with the magnitude of $\pm$ 20 cm, whilst the update frequency of localization is 20 Hz. Such error will be added to the vehicle plant localization.

Chapter 4

Comfort oriented model predictive control

Taking the vehicle model introduced in Chapter 3 as the prediction model, we formulate the path following as an optimization problem in MPC to minimize the tracking error between tracking signals and predicted output, as well as the control effort. In this chapter, we firstly introduce the MPC formulation for the baseline controllers, followed by the MPC with frequency shaped cost function. Due to the limitation of the linear bicycle model and the uncertainty brought by external disturbances, we use a disturbance observer (DOB) to compensate the modelling error. Lastly, we summarize the proposed methodology, as well as the baseline controllers that are adopted in the simulation.

4-1 Path following control

As Figure 1-1 indicates, the vehicle plant must follow a reference path with the effort of the MPC controller. Having a desired path described by a set of X and Y coordinates, we assume that a motion planning module computes a sequence of reference signals for the path following controller to follow, which are described by the lateral position and yaw angle, $y_{\text{ref}} = [\ Y_{\text{ref}} \quad \psi_{\text{ref}}\ ]^T$. In the path following module, the controller computes the commands that are required to track the given y_{ref}, where the commands usually refer to the steering angle.

4-2 Model predictive control

We rely on MPC to design our path following controller. MPC is an optimization-based control technique that relies on the prediction model and the optimizer. The prediction model refers to the dynamic model of process that is used to predict the future behavior of the plant over a predefined time window called prediction horizon N_p. An optimizer

computes a control input sequence that minimizes a cost function over the prediction horizon based on the current measurements from the plant, constraints and control objectives. The first element of this control input sequence is applied to the plant. In our case, the cost function is written as a quadratic programming (QP) problem. Thus, MPC optimizes the system for not only the current time step but also the future system behavior. Besides, the optimization also deals with the constraints on input, output and state, where the optimal control is found within the defined region. In the next sampling instant, the optimization will be repeated with new measurements. The MPC controller should compute the control input for current time step before the calculation of the next time step happens, which means that the computational time should be within the sampling time T_s of the system to accomplish real-time computation.

Discretize the linear dynamic bicycle model given as continuous-time state space in (3-9) and (3-10), the prediction model for MPC control is formulated in the form as in (4-1).

$$\begin{aligned} x(k+1) &= Ax(k) + Bu(k) \\ y(k) &= Cx(k) + Du(k) \end{aligned} \tag{4-1}$$

The MPC controller for path following can be described as in (4-2)

$$\begin{aligned} \underset{u}{\text{minimize}} \quad & J \\ \text{subject to} \quad & x_{\min} \leqslant x(k) \leqslant x_{\max}, \\ & u_{\min} \leqslant u(k) \leqslant u_{\max}, \\ & \Delta u_{\min} \leqslant \Delta u(k) \leqslant \Delta u_{\max} \end{aligned} \tag{4-2}$$

The cost function is the sum of: (i) the cost J_{tracking} that penalizes the tracking error e_y defined by (4-3), (ii) the cost $J_{\Delta u}$ that penalizes the increments of steering angle that defined by (4-4).

$$e_y(k) = y(k) - y_{\text{ref}}(k) \tag{4-3}$$

$$\Delta u(k) = u(k) - u(k-1) \tag{4-4}$$

In path following, we aim at reaching the final destination in time. Also, the precise tracking at each time step may not be feasible due to the system uncertainties. Instead of precisely tracking each point in the prediction horizon, we prefer to emphasize the tracking to the final destination within the horizon. Hence, we design a cost function that penalizes the tracking error at terminal state with weights higher than the other states within the horizon. The cost function also penalizes the increments of control effort, which help the vehicle get to the destination with smooth motion.

$$\begin{aligned} J &= J_{\text{tracking}} + J_{\Delta u} \\ &= \left[\sum_{i=1}^{N_p-1} e_y(k+i)^T a Q e_y(k+i) + e_y(k+N_p)^T Q e_y(k+N_p) \right] \\ &+ \sum_{i=0}^{N_p-1} \Delta u(k+i)^T R \Delta u(k+i) \end{aligned} \tag{4-5}$$

Besides, the prediction horizon N_p, weighting matrices Q and R , and the intermediate state tracking error penalty a are supposed to be tuned to find an optimal solution.

4-3 Frequency shaped model predictive control

As the lateral acceleration based comfort optimization will be included in the FSMPC scheme, the system output (3-10) is augmented with lateral acceleration a_y described by (3-6). The output of prediction model is therefore formulated as (4-6). As only a_y will be optimized regarding frequency, the output of prediction model is separated to two parts as in (4-7) and (4-8) for a clear notation.

$$\begin{bmatrix} Y \\ \psi \\ \hdashline a_y \end{bmatrix} = \left[\begin{array}{cccc} 0 & 0 & 1 & 0 \\ 0 & 0 & 0 & 1 \\ \hdashline -\frac{C_{\alpha f}+C_{\alpha r}}{mu} & \frac{l_r C_{\alpha r}-l_f C_{\alpha f}}{mu} & 0 & 0 \end{array}\right] \begin{bmatrix} v \\ r \\ Y \\ \psi \end{bmatrix} + \begin{bmatrix} 0 \\ 0 \\ \hdashline \frac{C_{\alpha f}}{m} \end{bmatrix} \delta \tag{4-6}$$

$$y = Cx \tag{4-7}$$

$$a_y = C_a x + D_a u \tag{4-8}$$

Having comfort optimization in the controller, the optimization function is extended with the cost for motion sickness J_{ms} and the cost for general discomfort J_{wd} for the purpose of minimizing the filtered acceleration $a_{y,\text{ms}}$ and $a_{y,\text{wd}}$ respectively.

$$J_{\text{FSMPC}} = J_{\text{tracking}} + J_{\Delta u} + J_{\text{ms}} + J_{\text{wd}} \tag{4-9}$$

The frequency dependent optimization for a_y can be written as the filtered acceleration in frequency domain with respect to motion sickness and general discomfort. We write motion sickness filter $F_{\text{ms}}(\omega)$ and general discomfort filter $F_{\text{wd}}(\omega)$ in one matrix. Then the comfort cost J_{comfort} is formulated as (4-10).

$$\begin{aligned} J_{\text{comfort}} &= J_{\text{ms}} + J_{\text{wd}} \\ &= \sum ||F_{\text{ms}}(\omega)a_y(\omega))||_2^2 Q_{a,\text{ms}} + \sum ||F_{\text{wd}}(\omega)a_y(\omega))||_2^2 Q_{a,\text{wd}} \\ &= \sum ||F(\omega)a_y(\omega))||_2^2 Q_a \end{aligned} \tag{4-10}$$

For the filter $F(\omega)$ which is described by a transfer function $F(\omega) = C_f(e^{j\omega}I - A_f)^{-1}B_f + D_f$, it can be written as a discrete-time filter regarding the sampling time T_s.

$$\begin{aligned} z(k+1) &= A_f z(k) + B_f a_y(k) \\ y_f(k) &= C_f z(k) + D_f a_y(k) \end{aligned} \tag{4-11}$$

We augment the prediction model with new state $z(k)$ and new output $y_f(k)$.

$$\begin{aligned}
\begin{bmatrix} x(k+1) \\ z(k+1) \end{bmatrix} &= \begin{bmatrix} A & 0 \\ B_f C_a & A_f \end{bmatrix} \begin{bmatrix} x(k) \\ z(k) \end{bmatrix} + \begin{bmatrix} B \\ B_f D \end{bmatrix} u(k) \\
\begin{bmatrix} y(k) \\ y_f(k) \end{bmatrix} &= \begin{bmatrix} C & 0 \\ D_f C_a & C_f \end{bmatrix} \begin{bmatrix} x(k) \\ z(k) \end{bmatrix} + \begin{bmatrix} C \\ D_f D_a \end{bmatrix} u(k)
\end{aligned} \tag{4-12}$$

Finally, J_{comfort} is rewritten in time domain and the FSMPC controller is formulated as follows.

$$\begin{aligned}
\underset{u}{\text{minimize}} \quad & J_{\text{FSMPC}} = J_{\text{tracking}} + J_{\Delta u} + J_{\text{comfort}} \\
& = \left[\sum_{i=1}^{N_p-1} e_y(k+i)^T a Q e_y(k+i) + e_y(k+N_p)^T Q e_y(k+N_p) \right] \\
& + \sum_{i=0}^{N_p-1} \Delta u(k+i)^T R \Delta u(k+i) + \sum_{i=1}^{N_p} y_f(k+i)^T Q_a y_f(k+i) \\
\text{subject to} \quad & x_{\min} \leqslant x(k) \leqslant x_{\max}, \\
& u_{\min} \leqslant u(k) \leqslant u_{\max}, \\
& \Delta u_{\min} \leqslant \Delta u(k) \leqslant \Delta u_{\max}
\end{aligned} \tag{4-13}$$

As we aim at improving comfort by optimizing both the $a_{y,\text{ms}}$ and $a_{y,\text{wd}}$, it would be the best solution to adopt the frequency weighting functions W_d and $W_{f,\text{lateral}}$ as $F_{\text{ms}}(\omega)$ and $F_{\text{wd}}(\omega)$ in the controller. However, due to the filter complexity, we should augment the prediction model with 14 states and two outputs for comfort optimization. This will also augment the computational requirements. In order to augment the controller with comfort optimization without largely increasing the system complexity, two simplified filters are adopted according to the discussion in Section 2-3 to penalize the undesired acceleration frequencies. The filters are simplified as two bandpass filters for motion sickness and general discomfort, where the pass bands are 0.03 - 0.2 Hz and 1- 2 Hz respectively. Only four states and two outputs are needed. Besides, it should be noted that the signals fall in the pass bands actually have higher penalties, since they are corresponding to higher magnitude.

4-4 Disturbance observer

As the tracking error and acceleration are optimized based on the prediction model described by (3-9) and (3-10), the controller performance is dependent on the modelling accuracy. Recall that we use a 2-DOF linear bicycle model as the prediction model, while the vehicle plant is a 9-DOF nonlinear multibody mode. The mismatch always exists due to the unmodelled system details and nonlinearity, which is especially significant when the slip angle is large. In addition, this study takes external disturbances into account, where the system uncertainties arise. These uncertainties are not able to be modelled in the prediction model and consequently increase the modelling error in the controller.

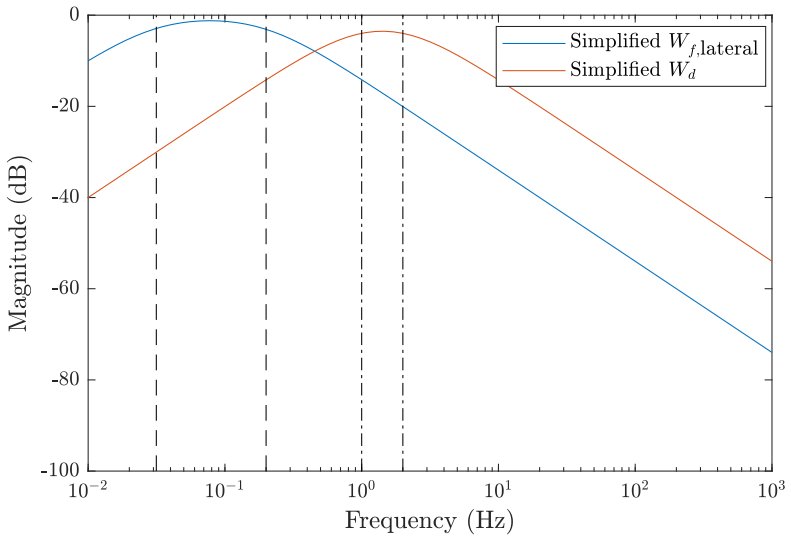

Figure 4-1: Comfort filters in FSMPC. The frequency range of interest for lateral motion sickness is indicated between the dash lines, for lateral general discomfort is indicated between the dash-dot lines.

In order to reduce such plant-model mismatch, a disturbance observer is applied to the controller as given in (4-14).

$$\begin{aligned} d(k) &= y_m(k) - y(k) \\ d(k) &= d(k) + d(k-1) \end{aligned} \tag{4-14}$$

The disturbance observer calculates the difference between measured output from vehicle plant and predicted output from the MPC controller, and the difference is applied to the prediction model as an additional term $d(k)$. Such mismatch is assumed constant at each time step over the prediction horizon.

$$y(k+1) = Cx(k) + Du(k) + d(k) \tag{4-15}$$

4-5 Proposed methodology

In order to tackle the comfort problem on path following control under disturbances, we propose the MPC controller with frequency dependent optimization on lateral acceleration, together with the disturbance observer described in Section 4-4 to mitigate the plant-model mismatch. The block diagram of proposed methodology is plot as in Figure 4-2. In the simulation presented in the next chapter, the performance of proposed FSMPC controller will be compared with the baseline controllers from the perspectives of tracking accuracy and driving comfort. The structure of the baseline controllers and the FSMPC controller differ from each other, are tabulated in Table 4-1.

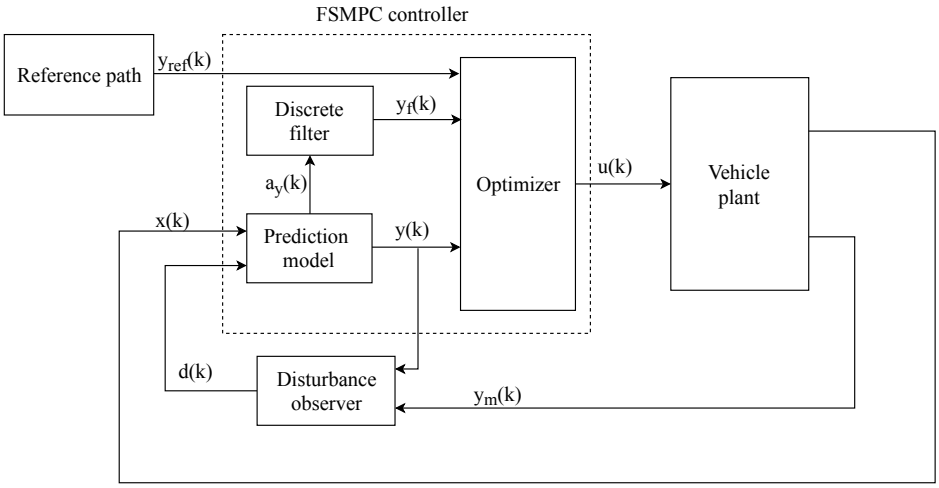

Figure 4-2: Proposed FSMPC controller structure.

Table 4-1: Controller structures in simulation.

Controller	Cost function	Disturbance observer
No control (NC)	$--$	Off
MPC-1	J_{tracking}	Off
MPC-2	$J_{\text{tracking}} + J_{\Delta u}$	Off
MPC+DOB	$J_{\text{tracking}} + J_{\Delta u}$	On
FSMPC+DOB	$J_{\text{tracking}} + J_{\Delta u} + J_{\text{ms}} + J_{\text{wd}}$	On

Chapter 5

Simulation and results

In order to tune and evaluate the proposed FSMPC controller, we use a high fidelity 9-DOF vehicle plant to simulate the vehicle behaviour in three different scenarios. We compared the performance of controllers described in Table 4-1. After introducing the simulation setup and the scenarios, the results are presented regarding the tracking error and comfort indices,that are, motion sickness index $a_{y,\mathrm{ms}}$ in 2-3 and general discomfort index $a_{y,\mathrm{wd}}$ in (2-1).

5-1 Setup

We simulated a Toyota Prius model in Matlab/Simulink. The proposed controller for path tracking in Chapter 4 is used to control a multibody vehicle plant to follow a desired reference trajectory designed by a well-designed path planner. As this project is focused on the lateral performance, the forward velocity is assumed constant in all the tests without acceleration/deceleration, in the range of 20 - 120 km/h.

5-1-1 Vehicle plant

The plant model has 9 degrees of freedom, that are, three translational motion (longitudinal, lateral, vertical), three rotational motion (roll, pitch, yaw) of the vehicle, and the suspension behaviour. The tire behaviour is modelled by the Delft Tire model based on Magic Formula, in the combined slip mode with relaxation behaviour. The longitudinal speed is controlled by a PID controller whilst the lateral motion is controlled by our proposed controllers in Table 4-1. Further, the Ackermann geometry is taken into account as apart of steering system modelling.

5-1-2 Controller settings

The QP problem that comes from our MPC design is solved by Matlab's `quadprog` function. The following settings will be applied on the controller, where the constraints on steering

angle and steering rate are determined according to the steering limits. Besides, since the FSMPC controller will make balance between tracking accuracy and motion comfort, the constraints for lateral tracking error of 1 m is applied to avoid the possible large deviation (enter the side lane) and instability over the prediction horizon at disturbance rejection in such trade-offs.

- Sampling time: $T_s = 0.05$ s.
- Prediction horizon: $N_p = 20$.
- Steering angle constraints: $-30 \text{ deg} \leqslant \delta \leqslant 30 \text{ deg}$,
  Steering rate constraints: $-20 \text{ deg/s} \leqslant \delta \leqslant 20 \text{ deg/s}$.
- Lateral deviation constraints for FSMPC: -1 m $\leqslant Y_{\text{ref}} - Y \leqslant 1$ m

Hence, the prediction time is 1 s in total. The tunable parameters for the path following controller are the weighting matrix Q and coefficient a for tracking performance, matrix R for control effort, and Q_a for driving comfort. There are two weighting factors in Q_a for motion sickness and general discomfort respectively. The penalties given by Q and R are fixed for all the test velocities, whilst a gain scheduling scheme for Q_a is developed to accommodate the different frequency response to the disturbances at different forward speeds. The choice of MPC parameters is explained in Appendix A.

5-2 Scenarios

In order to show the steer controller performance from the perspective of driving comfort, disturbance rejection and tracking performance, three simulation scenarios are tested.

- **Scenario 1: Straight drive**

  The straight driving manoeuvre with disturbances is adopted to test the comfort optimization performance of the controller, alongside with the disturbance rejection ability. Assuming the vehicle plant is driving on a straight road for 30 seconds, three typical external disturbances are applied to the simulation, the modelling details of which were described in Section 3-2. The disturbances are applied to the manoeuvre separately, following by a combination of all of them. As friction changes do not have observable impact on straight drive with respect to both tracking accuracy and passenger comfort, we only consider the friction changes in combination with the other disturbances to get as much noise as possible. In summary, we consider three cases in total:

  - Case 1: Crosswind
    The crosswind is modelled as a wind gust of 10 m/s acting laterally on the vehicle at time t = 1 s, where the wind speed remains constant afterwards.
  - Case 2: Sensor noise
    The sensor noise is added to the vehicle localization on the Y axis all along the manoeuvre.

– Case 3: Combined disturbances

With the same magnitude as the former cases, the crosswind impacts the vehicle at time t = 1 s, the change of road surface from dry asphalt to icy condition happens at time t = 2 s, and the sensor noise is applied on the vehicle localization system all the time.

In the straight driving scenario, the reference signals lateral position Y_{ref} and yaw angle ψ_{ref} for tracking are both zero along the manoeuvre.

- **Scenario 2: Double lane change**

ISO 3888 adopts double lane change (Figure 5-1) to evaluate the steering system performance under emergency situations, where the vehicle needs to switch to the side lane and switch back without knocking down the cones. In this study, the double lane change manoeuvre is used to guarantee the controller can still handle the emergency situation while driving comfort is taken into account in FSMPC.

The controller should track the reference signals as described in (5-1) and (5-2) so that the vehicle plant can complete the double lane change manoeuvre.

$$Y_{ref} = \begin{cases} 0 & X < 15 \\ \frac{3.5}{2}\left\{1 - \cos\left[\frac{\pi}{30}(X-15)\right]\right\} & 15 \leqslant X < 45 \\ 3.5 & 45 \leqslant X < 70 \\ \frac{3.5}{2}\left\{1 + \cos\left[\frac{\pi}{30}(X-70)\right]\right\} & 70 \leqslant X < 95 \\ 0 & 95 \leqslant X < 120 \end{cases} \tag{5-1}$$

$$\psi_{ref} = \begin{cases} 0 & X < 15 \\ \arctan\left\{\frac{3.5\pi}{60}\sin\left[\frac{\pi}{30}(X-15)\right]\right\} & 15 \leqslant X < 45 \\ 0 & 45 \leqslant X < 70 \\ \arctan\left\{\frac{3.5\pi}{60}\sin\left[\frac{\pi}{30}(X-70)\right]\right\} & 70 \leqslant X < 95 \\ 0 & 95 \leqslant X < 120 \end{cases} \tag{5-2}$$

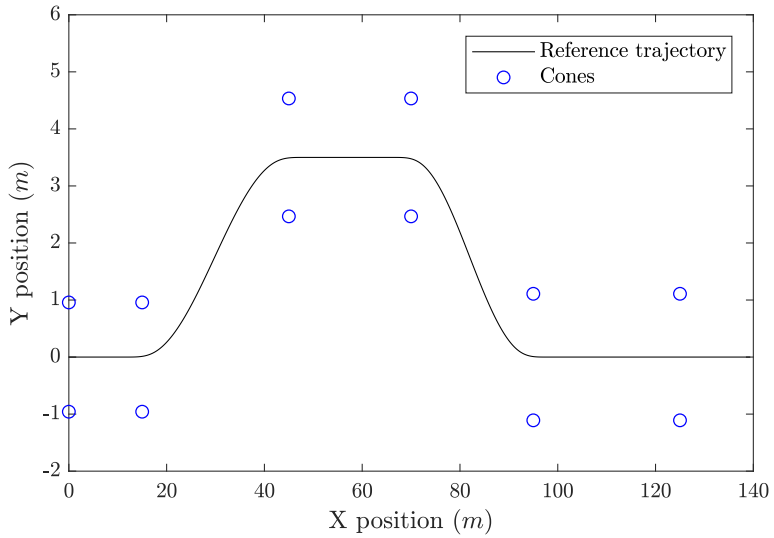

Figure 5-1: Double lane change reference.

- **Scenario 3: Sinusoidal trajectory**

  The acceleration frequency of a sinusoidal trajectory can be defined by specifying the oscillation frequency of the trajectory. Therefore a well-designed sinusoidal trajectory can easily excite the driving discomfort with specific frequency as introduced in Section 2-3. In this simulation, the vehicle having forward velocity of 60 km/h will follow the sinusoidal track that oscillates with the amplitude of 3 m and excites the acceleration frequency around 0.2 Hz, after an entry of 5 seconds (Figure 5-2). The effect of disturbance observer to the proposed controller and the effect of weighting factor Q_a on balancing vehicle tracking performance with driving comfort will be discussed based on this simulation results.

$$Y_{\text{ref}} = \begin{cases} 0 & t < 5 \\ 3\sin\left[0.4\pi(t-5)\right] & t > 5 \end{cases} \tag{5-3}$$

$$\psi_{\text{ref}} = \begin{cases} 0 & t < 5 \\ \arctan\left\{\dfrac{1.2\pi}{60}\cos\left[0.4\pi(t-5)\right]\right\} & t > 5 \end{cases} \tag{5-4}$$

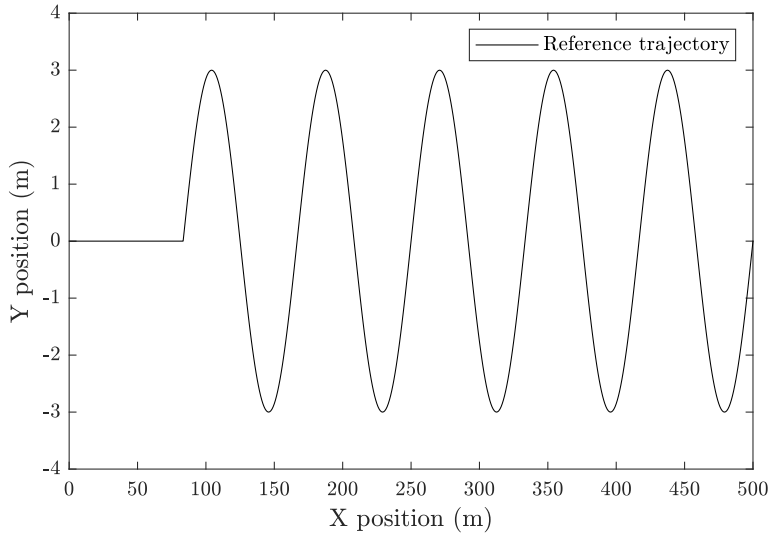

Figure 5-2: Sinusoidal trajectory reference at forward speed 60 km/h.

5-3 Results

5-3-1 Disturbance rejection

The disturbance rejection experiment conducted on the straight drive simulation shows that the FSMPC controller can enhance the vehicle lateral motion comfort without largely increasing the tracking error, compared to the baseline controllers. The details of controller performance are tabulated in Appendix C, where the tracking performance is evaluated by the lateral deviation, and the passenger comfort is evaluated by index $a_{y,\mathrm{ms}}$ and index $a_{y,\mathrm{wd}}$. Besides, the following section analyses and explains the simulation results.

Case 1: Crosswind The summary of tracking and comfort performance of the tested controllers in the velocity range of 20 - 120 km/h is plotted as in Figures 5-3, 5-4, 5-5 and 5-6.

From the presented simulation results, it is found that the tested controllers except MPC-1 do not generate uncomfortable motions under the crosswind of 10 m/s, since all the values of $a_{y,\mathrm{ms}}$ and $a_{y,\mathrm{wd}}$ are kept under 0.0315 m/s^2, which are very small for human perception. The exception is found on controller MPC-1, where the cost function only penalizes the tracking accuracy.

Since the cost function does not minimize the control effort while being very sensitive to the tracking error, the steer input computed by MPC-1 is overly aggressive to correct the tracking error, especially under the unmodelled disturbance. As the consequences, the controller is unstable. The real trajectory shows the persistent oscillations around the reference trajectory

($y_{\text{ref}} = 0$). Such oscillations brought by the controller cause extra discomfort, especially from the perspective of general discomfort, as the values of $a_{y,\text{ms}}$ and $a_{y,\text{wd}}$ shown in Figure 5-3.

Compare all the simulation results from 20 to 120 km/h for no steer control under crosswind, it is found that the lateral deviation accumulates to some large numbers (over 1 m) as the growth of time, as the consequences of side force F_w and side moment M_w. Besides, as the response to constant side wind, the lateral acceleration rises to a certain value in a short time and then recover, it is the reason for the low values of comfort indices.

Notice that the performance on both tracking and comfort of all simulation velocities are very similar between MPC-2 and MPC+DOB, it indicates that the effect of disturbance observer is small when doing straight driving under crosswind. From the perspective of simulation manoeuvre, the straight drive does not generate too much plant-model mismatch, as the forward velocity is constant over the simulation, whilst the unmodelled system nonlinearity happens in the lateral direction is usually remarkable during cornering but not straight driving scenario. On the other hand, the disturbance brought by crosswind at 10 m/s does not have significant impact on tracking error, the space for disturbance correction is therefore restricted, although the MPC+DOB scheme always shows slightly less lateral error than MPC-2 all the time along the simulation (Figure 5-4). Further, their tracking and comfort performance are both better than MPC-1, which indicates that the penalty on steering effort reduces the sensitivity of controller to tracking error, and hence the controller is more stable.

When the cost function is extended with comfort penalty on lateral acceleration, it is found that FSMPC controller shows worse performance than MPC-2 and MPC+DOB on both the tracking and comfort, apart from the general discomfort index $a_{y,\text{wd}}$ over 100 km/h. For the low forward velocity (20 - 60 km/h) under crosswind, no Q_a tuning can be found to stabilize the trajectory faster than the baseline controllers MPC-2 and MPC+DOB. The FSMPC at 20 km/h has very similar performance to MPC-2 and MPC+DOB, while the drift is slightly higher (Figure 5-4). As for 40 and 60 km/h, both the steady error and duration of damped oscillation raise, whilst the oscillation is slower. Such effect can be the result of frequency dependent optimization. The controller tries to reject the acceleration frequency in the range of 0.03 - 0.2 Hz and 1 - 2 Hz. The acceleration frequency response to steering motion usually lays in the range of 0 - 2 Hz. The steer controller actually tries to accumulate the acceleration to the frequency between 0.2 to 1 Hz. It is possible that such frequency response causes poor damping for the controller at low forward speed under crosswind. Meanwhile, the FSMPC successfully stabilize the vehicle plant faster than any other baseline controllers with acceptable tracking error at the forward velocity higher than 80 km/h, as indicated in Figure 5-4. Although the vehicle oscillates less with FSMPC, its comfort indices do not decrease due to the higher drift presented, which increases the instantaneous acceleration at the beginning when the crosswind occurs at t = 1 s (Figure 5-5, 5-6). It is found that the higher penalties on frequency weighted acceleration can further improve the comfort performance and reduce the damped oscillation at driving speed 80 - 120 km/h, but simultaneously increases the tracking error with higher drift. Compare to the lateral deviations of the baseline controllers that are always stay lower than 0.03 m, the FSMPC controller is tuned to improve the comfort as much as possible while keeping the drift below 0.1 m.

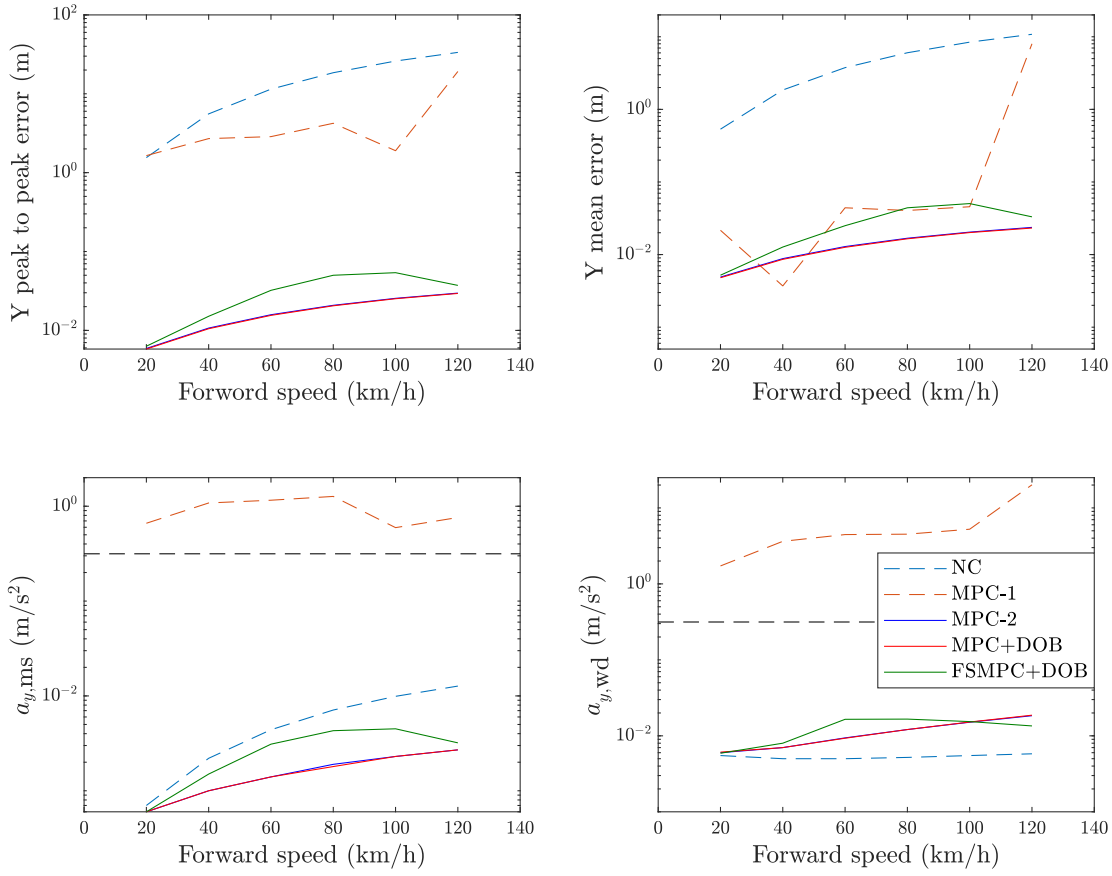

Figure 5-3: Tracking and comfort summary for disturbance rejection of crosswind. Comfort threshold is indicated by the dash line.

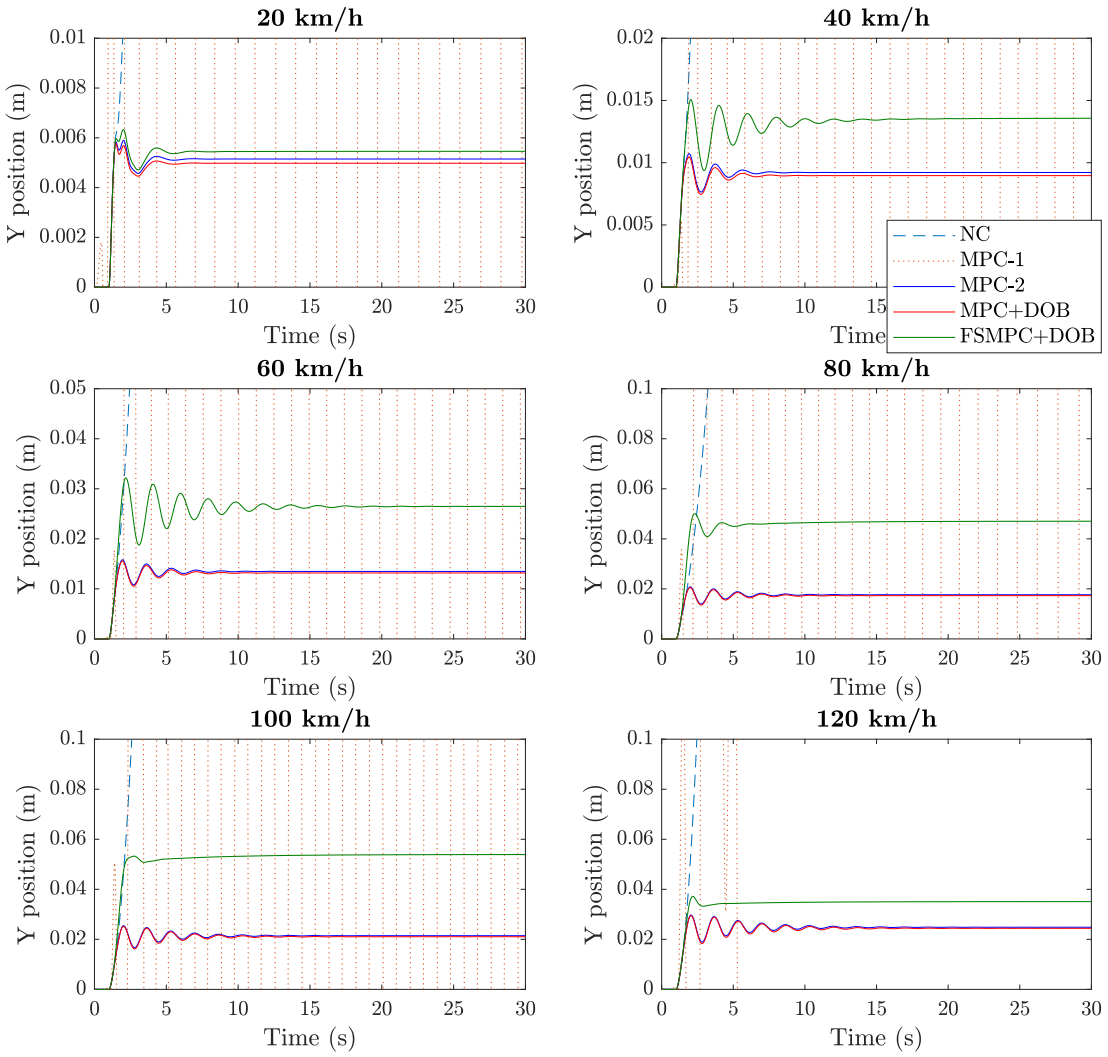

Figure 5-4: Lateral deviation for disturbance rejection of crosswind at forward speed 20 - 120 km/h.

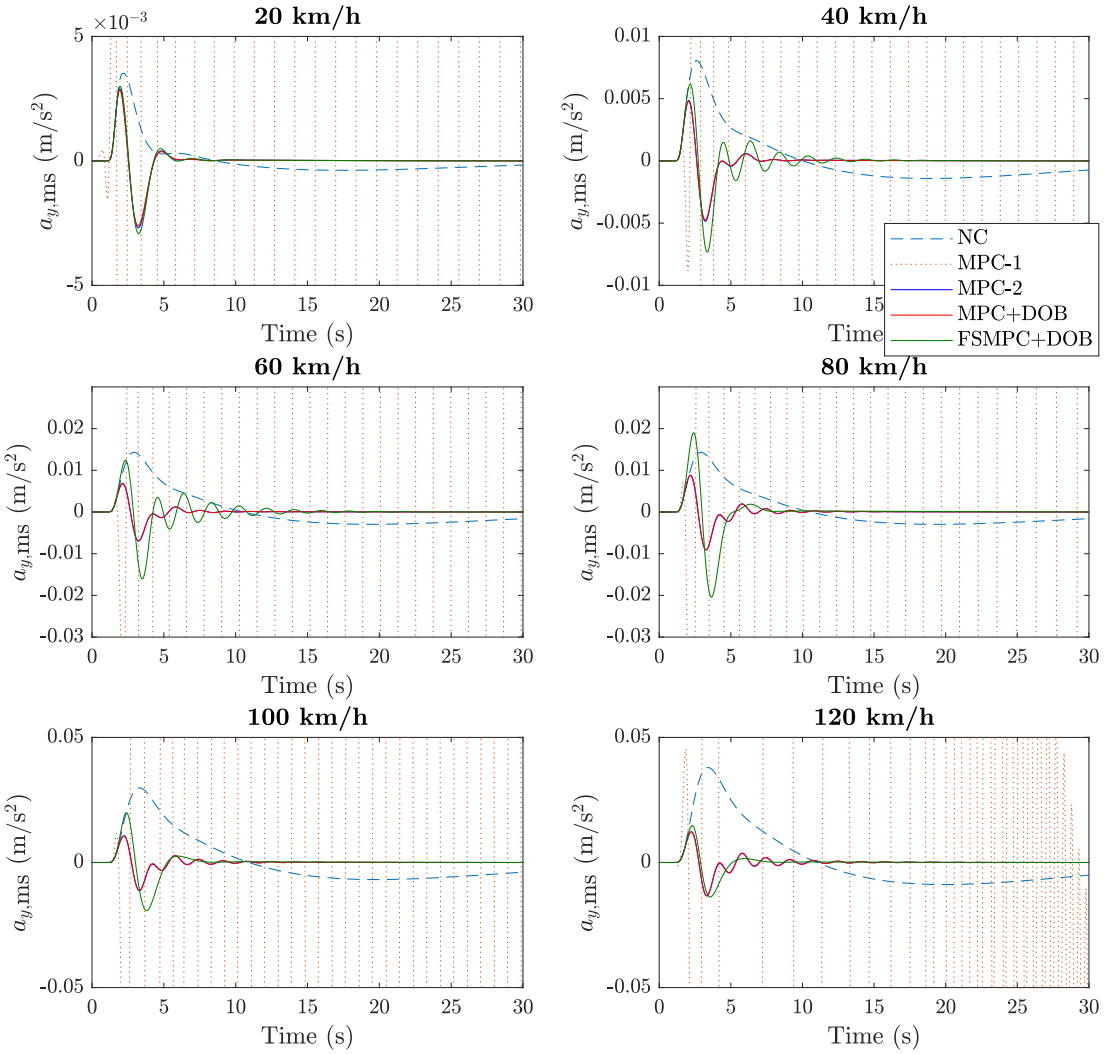

Figure 5-5: $W_{f,\mathrm{lateral}}$ filtered acceleration history for disturbance rejection of crosswind at forward speed 20 - 120 km/h.

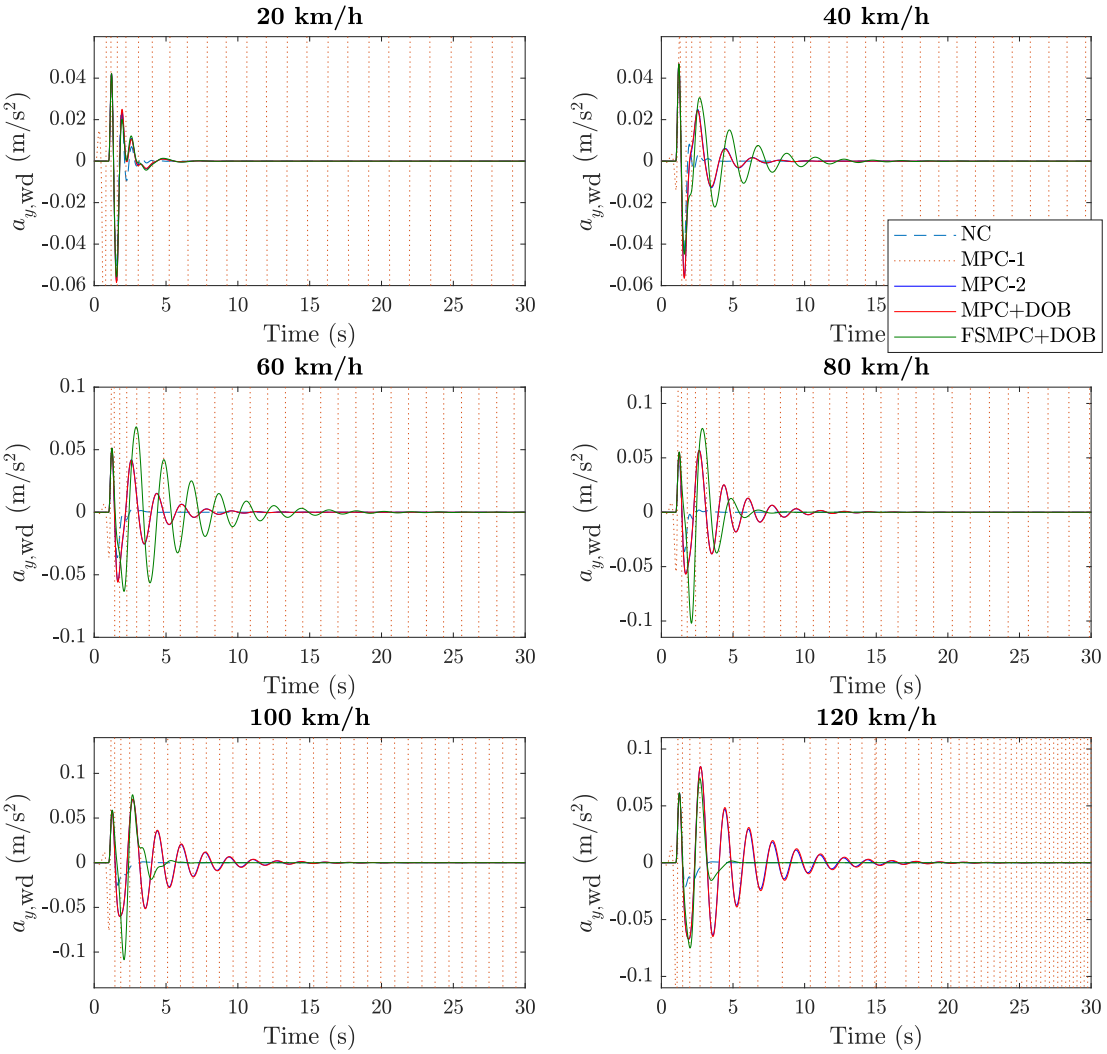

Figure 5-6: W_d filtered acceleration history for disturbance rejection of crosswind at forward speed 20 - 120 km/h.

Table 5-1: Improvement of FSMPC controller to baseline controllers on motion sickness index $a_{y,\mathrm{ms}}$ for disturbance rejection of crosswind.

Forward speed (km/h)	No control	MPC-1	MPC-2	MPC+DOB
20	15.01%	99.90%	(6.26%)	(8.85%)
40	34.26%	99.87%	(30.87%)	(32.21%)
60	28.79%	99.73%	(54.55%)	(55.15%)
80	38.59%	99.66%	(57.16%)	(57.51%)
100	54.12%	99.24%	(49.88%)	(50.08%)
120	74.68%	99.58%	(16.77%)	(16.70%)

* $(\cdot)$ indicates the corresponding baseline controller has smaller comfort index, the improvement is found in reverse.

Table 5-2: Improvement of FSMPC controller to baseline controllers on general discomfort index $a_{y,\mathrm{wd}}$ for disturbance rejection of crosswind.

Forward speed (km/h)	No control	MPC-1	MPC-2	MPC+DOB
20	6.67%	99.66%	2.71%	3.94%
40	(37.06%)	99.78%	(11.92%)	(11.97%)
60	(69.56%)	99.63%	(43.28%)	(43.50%)
80	(68.61%)	99.63%	(26.90%)	(26.84%)
100	(64.40%)	99.71%	(1.50%)	(0.74%)
120	(57.25%)	99.93%	26.82%	27.94%

* $(\cdot)$ indicates the corresponding baseline controller has smaller comfort index, the improvement is found in reverse.

Case 2: Sensor noise Since the localization error from sensor noise is a disturbance coming from the automated driving system itself, no further tracking error occurs if no control input is computed based on the inaccurate localization. The simulation without MPC steer control is therefore eliminated here, whilst the tracking and comfort performance of other controllers are described in Figure 5-7, 5-8, 5-9 and 5-10.

Similar to the results presented in the crosswind rejection, MPC-1 shows the worst performance regarding both tracking and comfort. With the uncertainties that are not able to be included in the prediction model, the unweighted steer input results in vehicle oscillation around the reference path, where the lateral deviation accumulates both the tracking and localization error. Further, the persistent oscillation with high acceleration provokes remarkable motion sickness and general discomfort for all simulation velocities.

Including the steering penalty in cost function largely reduce the fast shift of steering angle and the corresponding oscillation of the vehicle plant. Hence, the largely decreases on tracking error and motion discomfort are found on the MPC-2 and MPC+DOB controllers. Although the MPC-2 and MPC+DOB still have very similar performance, what different from the crosswind rejection is that the controller with disturbance observer always has slightly larger tracking error than the MPC controller without disturbance observer. The disturbance observer corrects the prediction model based on the discrepancies between plant measurement and model prediction, which requires the measurement to be precise with respect to the real plant state. On the contrary, the disturbance observer brings incorrect information to the prediction model and therefore has chance to enlarge the prediction inaccuracy when the measurement itself is not precise.

As for the FSMPC controller, its peak to peak error is quite close to the errors of MPC-2 and MPC+DOB control scheme, with the difference around $\pm$ 0.05 m. The slightly larger mean error implies that instead of baseline controllers that only aims at correcting the tracking error, the FSMPC controller that takes comfort into account is willing to compensate the vehicle tracking vibration by lateral deviation. The FSMPC controller shows a good rejection to motion sickness at the velocity higher than 60 km/h, where the largest improvement is found at 100 km/h, which is over 40% compared to both MPC-2 and MPC+DOB (Table 5-3). As for general discomfort, the value of $a_{y,\mathrm{wd}}$ is similar to MPC-2 and MPC+DOB in the velocity range of 20 - 40 km/h, whilst Table 5-4 indicates that the obvious improvements are found at higher velocities up to over 50% at 80 - 120 km/h. The comfort improvement at low velocities (20 - 40 km/h) is limited by the poorly damped controller response to crosswind as discussed in last section and shown in Figure 5-4. As indicated in Figure 5-9 and 5-10, for velocity higher than 60 km/h, the comfort improvement of FSMPC is accomplished by minimizing the value of filtered lateral acceleration. The output trajectory is therefore smoother than the outputs of baseline controllers (Figure 5-8).

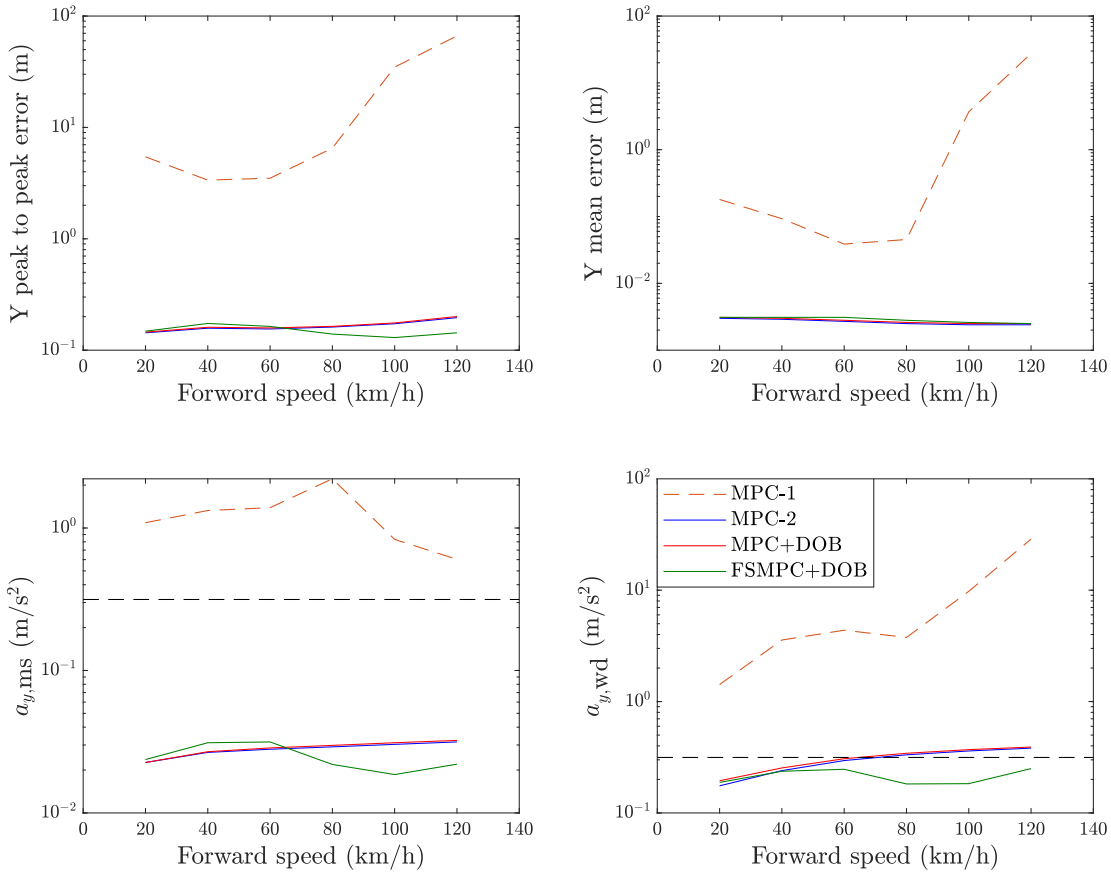

Figure 5-7: Tracking and comfort summary for disturbance rejection of sensor noise. Comfort threshold is indicated by the dash line.

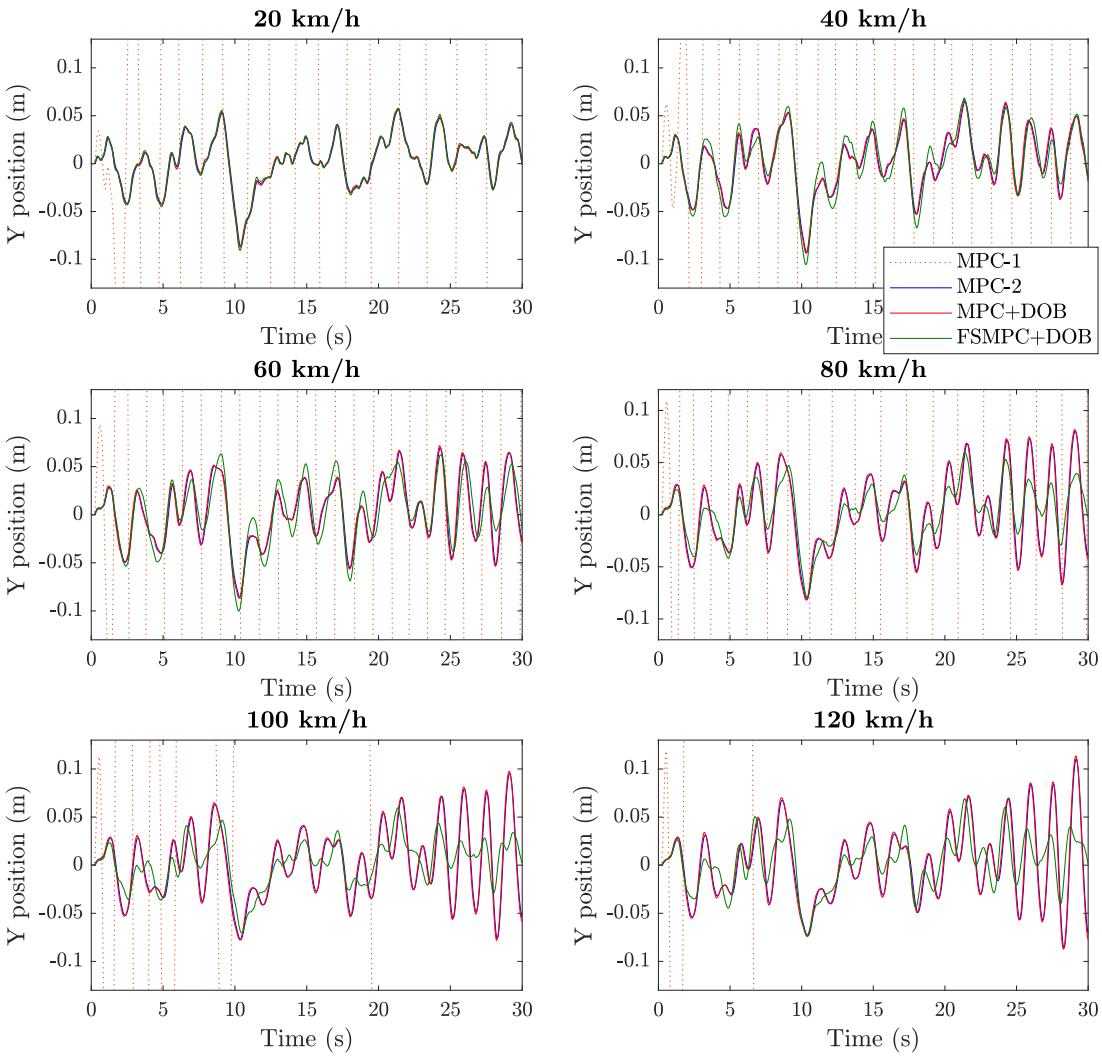

Figure 5-8: Lateral deviation at disturbance rejection of sensor noise at forward speed 20 - 120 km/h.

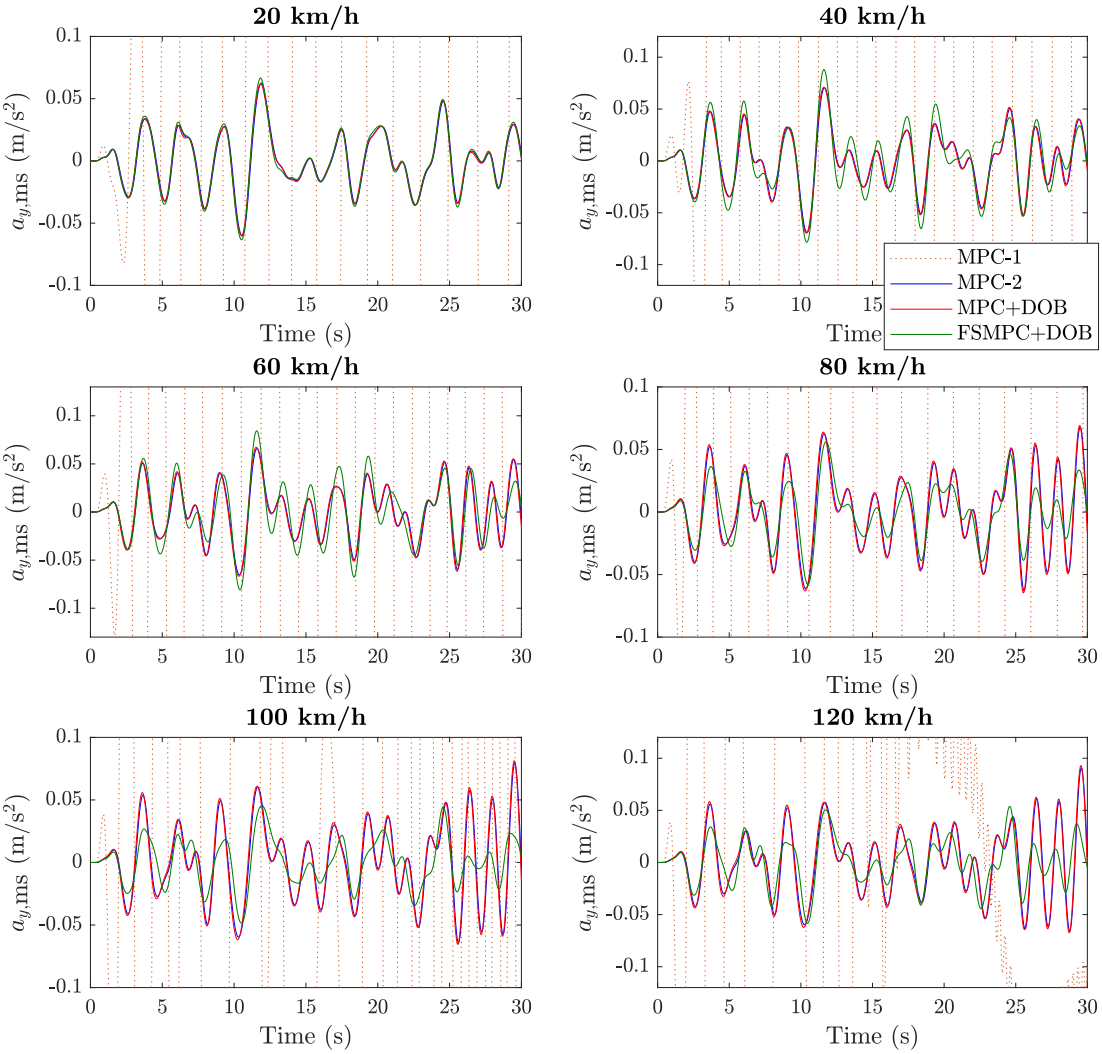

Figure 5-9: $W_{f,\mathrm{lateral}}$ filtered acceleration history for disturbance rejection of sensor noise at forward speed 20 - 120 km/h.

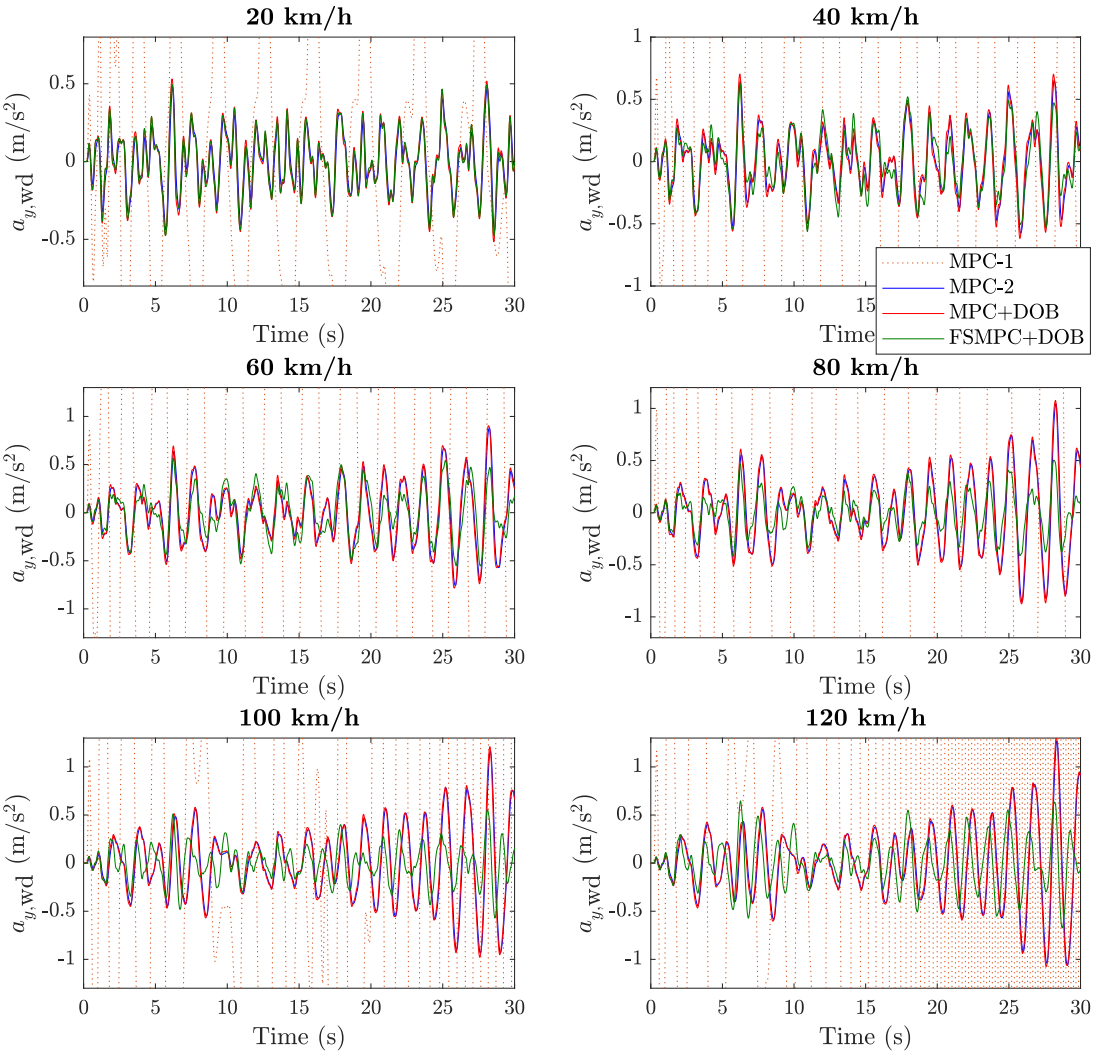

Figure 5-10: W_d filtered acceleration history at disturbance rejection of sensor noise at forward speed 20 - 120 km/h.

Table 5-3: Improvement of FSMPC controller to baseline controllers on motion sickness index $a_{y,\mathrm{ms}}$ for disturbance rejection of sensor noise.

Forward speed (km/h)	MPC-1	MPC-2	MPC+DOB
20	97.82%	(4.75%)	(4.93%)
40	97.66%	(14.36%)	(13.33%)
60	97.73%	(11.10%)	(9.25%)
80	99.01%	24.86%	26.71%
100	97.76%	38.45%	40.09%
120	96.35%	30.06%	31.96%

* $(\cdot)$ indicates the corresponding baseline controller has smaller comfort index, the improvement is found in reverse.

Table 5-4: Improvement of FSMPC controller to baseline controllers on general discomfort index $a_{y,\mathrm{wd}}$ for disturbance rejection of sensor noise.

Forward speed (km/h)	MPC-1	MPC-2	MPC+DOB
20	86.78%	(6.80%)	3.42%
40	93.37%	1.32%	6.65%
60	94.36%	16.48%	19.61%
80	95.17%	45.27%	46.97%
100	98.12%	49.14%	50.50%
120	99.13%	34.48%	35.94%

* $(\cdot)$ indicates the corresponding baseline controller has smaller comfort index, the improvement is found in reverse.

Case 3: Combined disturbances The simulation of vehicle response to combined disturbances without MPC control is also eliminated in this case, since its performance will be consistent to the no control case for crosswind rejection. Here, the sensor noise does not affect tracking accuracy as explained in last section, while no error from unmodelled tire nonlinearity at low friction will be introduced to the vehicle plant from MPC controller. Therefore, the lateral deviation only accumulates over time to certain large value as the consequences of the constant F_w and M_w exerted by crosswind, while the values of comfort indices $a_{y,\mathrm{ms}}$ and $a_{y,\mathrm{wd}}$ are quite small.

As indicated in Figure 5-11, the largest lateral error is found with controller MPC-1. The MPC-1 controller with our tuning scheme but drops the penalty on steer input loses control to the vehicle on the straight drive scenario with combined disturbances. The outstanding tracking error and passenger discomfort can both be found in the simulation.

Similar to the disturbance rejection simulation of crosswind and sensor noise, the controller MPC-2 and MPC+DOB show some similar performance regarding tracking and comfort, while the penalty on steer input stabilizes the controller to a large extent and therefore reduces both tracking error and motion discomfort, compared to MPC-1.

The improvements on general discomfort by FSMPC are found at all tested velocities (Table 5-6), especially for the velocity higher than 40 km/h. The motion sickness improvements at forward velocity from 80 to 120 km/h are around 30% (Table 5-5), while at lower speed the $a_{y,\mathrm{ms}}$ value of FSMPC is higher than MPC-2 and MPC+DOB, which is again due to limits of controller response to crosswind. Compare the tracking error to comfort performance in Figure 5-11, it it noticed that the tracking error is large when the comfort indices are relatively small, which indicates that the controller sacrifices the tracking accuracy to improve driving comfort. It is also found at Figure 5-12 at velocities higher than 60 km/h. Instead of the trajectory that oscillates around reference at $Y = 0$, the relatively more comfortable path generated by FSMPC controller is smoother, while deviating from the reference path with drift. Such deviation is the composition of the vehicle drift response to crosswind and friction drop, as well as the smooth response to sensor noise. Further, both the W_d and $W_{f,\mathrm{lateral}}$ filtered acceleration histories show that the FSMPC optimizes acceleration with respect to its corresponding frequency, whose values of $a_{y,\mathrm{ms}}$ and $a_{y,\mathrm{wd}}$ are always smaller than the baseline controllers (Figure 5-13, 5-14).

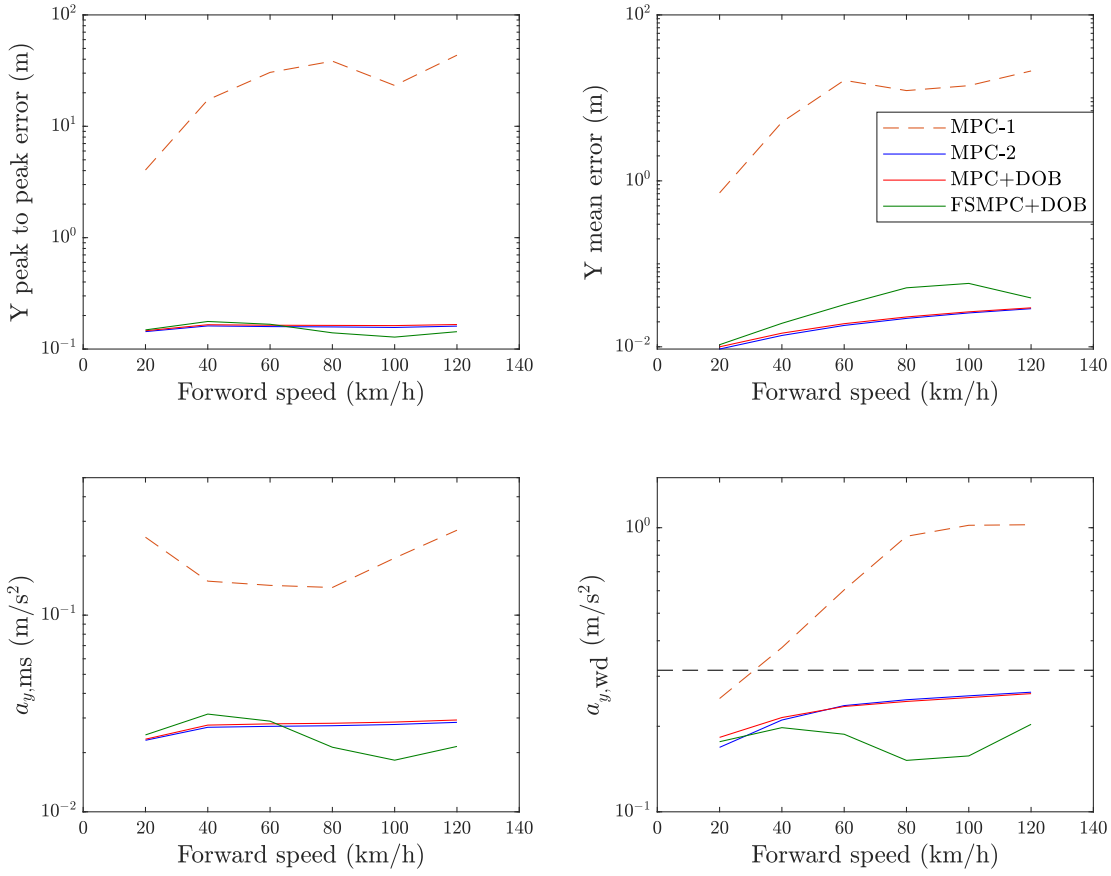

Figure 5-11: Tracking and comfort summary for disturbance rejection of combined disturbances. Comfort threshold is indicated by the dash line.

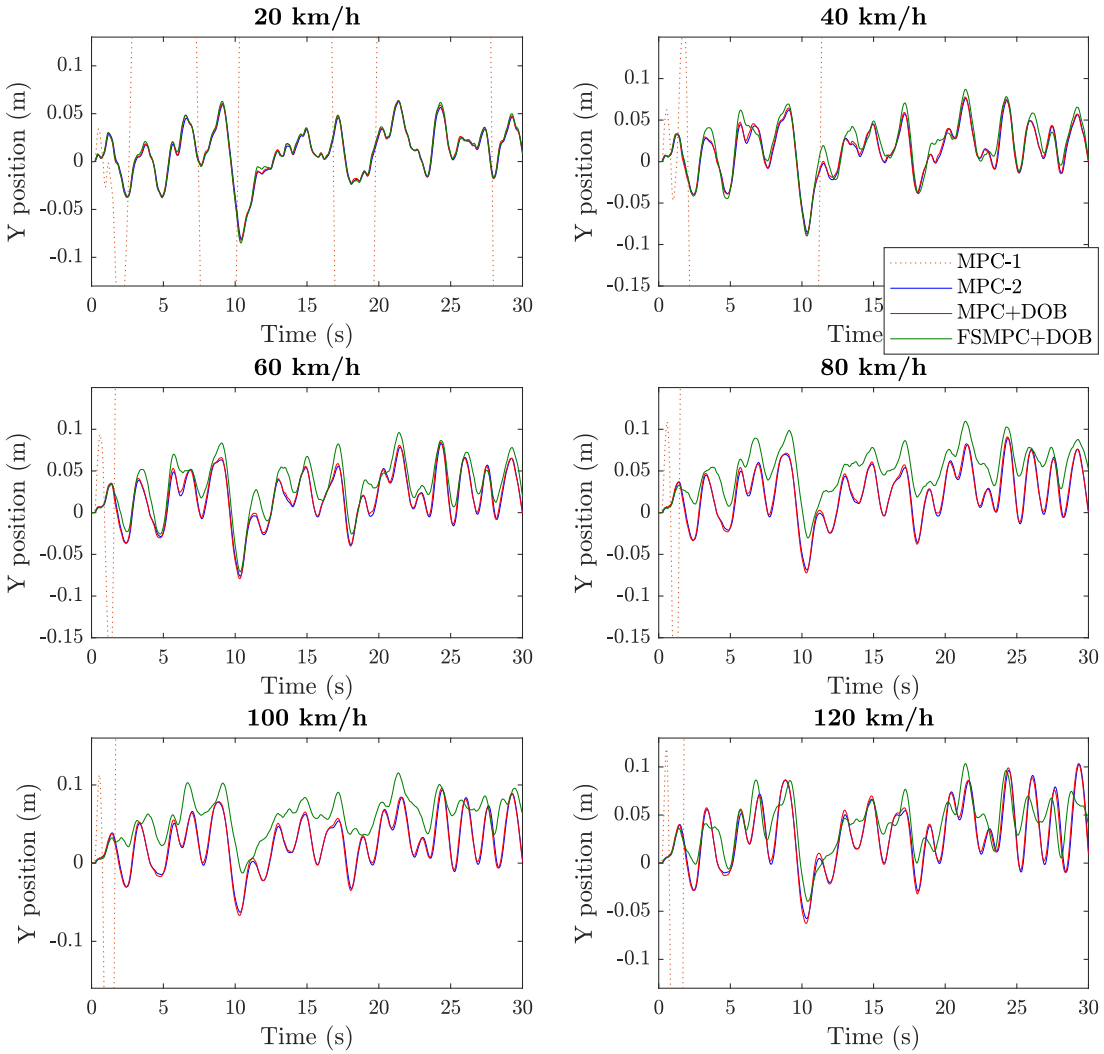

Figure 5-12: Lateral deviation at disturbance rejection of combined disturbances at forward speed 20 - 120 km/h.

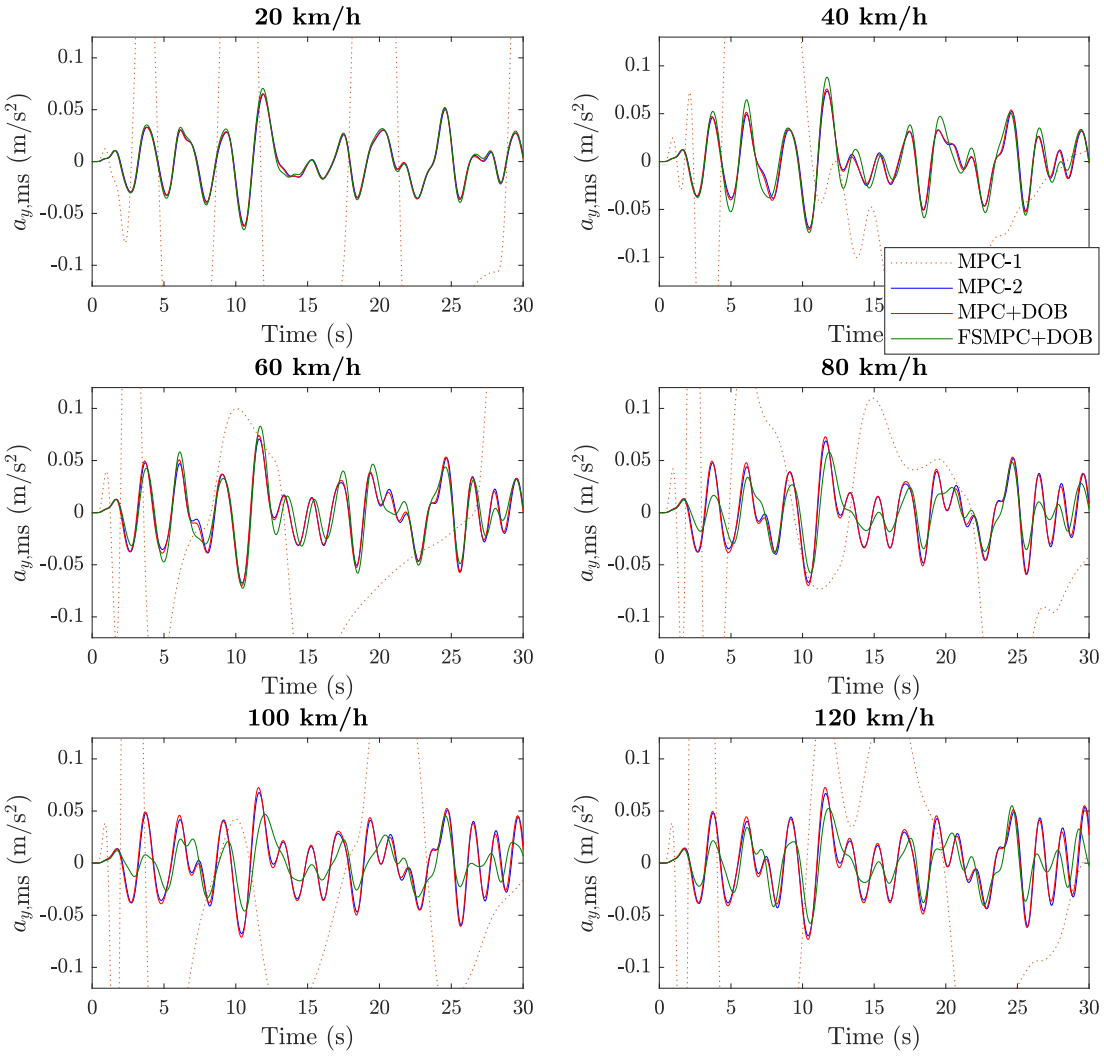

Figure 5-13: $W_{f,\mathrm{lateral}}$ filtered acceleration history for disturbance rejection of combined disturbances at forward speed 20 - 120 km/h.

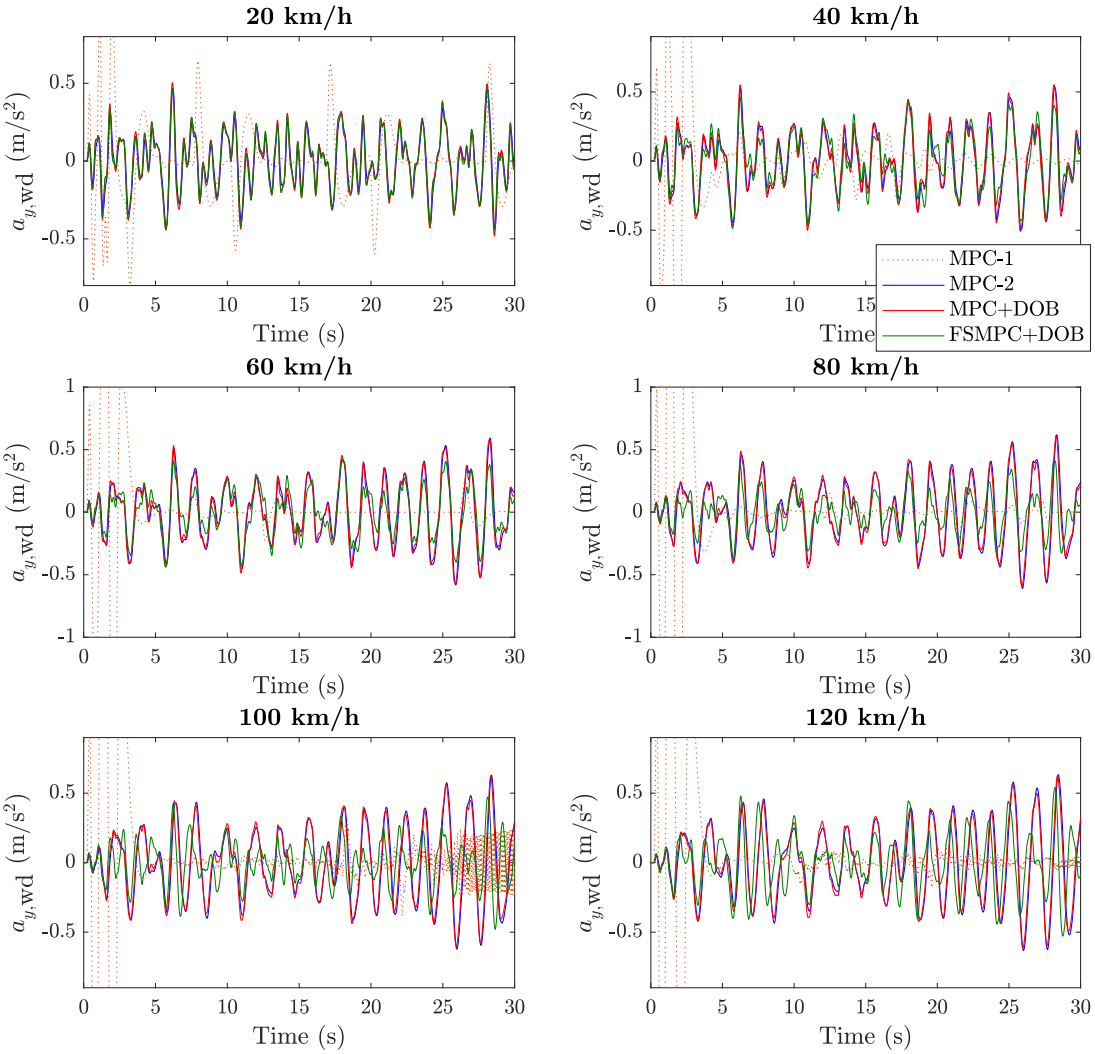

Figure 5-14: W_d filtered acceleration history at disturbance rejection of combined disturbances at forward speed 20 - 120 km/h.

Table 5-5: Improvement of FSMPC controller to baseline controllers on motion sickness index $a_{y,\mathrm{ms}}$ for disturbance rejection of combined disturbances.

Forward speed (km/h)	MPC-1	MPC-2	MPC+DOB
20	90.11%	(6.25%)	(5.01%)
40	78.89%	(14.34%)	(12.10%)
60	79.57%	(5.99%)	(3.31%)
80	84.60%	22.24%	24.43%
100	90.64%	34.18%	36.06%
120	92.04%	24.45%	26.63%

* $(\cdot)$ indicates the corresponding baseline controller has smaller comfort index, the improvement is found in reverse.

Table 5-6: Improvement of FSMPC controller to baseline controllers on general discomfort index $a_{y,\mathrm{wd}}$ for disturbance rejection of combined disturbances.

Forward speed (km/h)	MPC-1	MPC-2	MPC+DOB
20	29.55%	(4.45%)	3.45%
40	47.72%	5.98%	7.86%
60	68.95%	20.69%	20.11%
80	83.73%	38.83%	37.96%
100	84.57%	38.54%	37.67%
120	80.16%	22.91%	22.04%

* $(\cdot)$ indicates the corresponding baseline controller has smaller comfort index, the improvement is found in reverse.

5-3-2 Emergency handling

Apart from following a comfortable and smooth trajectory even in the environment full of disturbances, we also expect that the controller is able to handle the emergency situation without safety issue. An example of tracking-comfort trade-offs in path following is found in the crosswind disturbance rejection scenario between the no control case and MPC-1, where a "lazy" control avoids uncomfortable motion but generates large deviation, whilst a controller with fast response produces discomfort vibration and even an unstable tracking. Even though we have had a controller that is comfortable with less sensitive response to uncertainties, it may also have lazy response to other situations such as the emergency situation. In the emergency situation, a dull steer response may not avoid the obstacles. The regulation of lateral acceleration in FSMPC can also reduce the flexibility of steer response. In order to prevent such situation, the simulation of a double lane change is performed to test and ensure the emergency handling ability of the proposed controller.

As the results shown in Figure 5-15, the FSMPC controller can pass the double lane change at all experimental velocities. For the velocity from 20 to 60 kn/h, FSMPC controller is able to have similar performance with the baseline controllers without comfort weighting. For the higher velocities from 80 to 120 km/h, when the Q_a has more space to tune, the extra comfort

term in MPC helps to stabilize the damped trajectory computed by the baseline controllers.

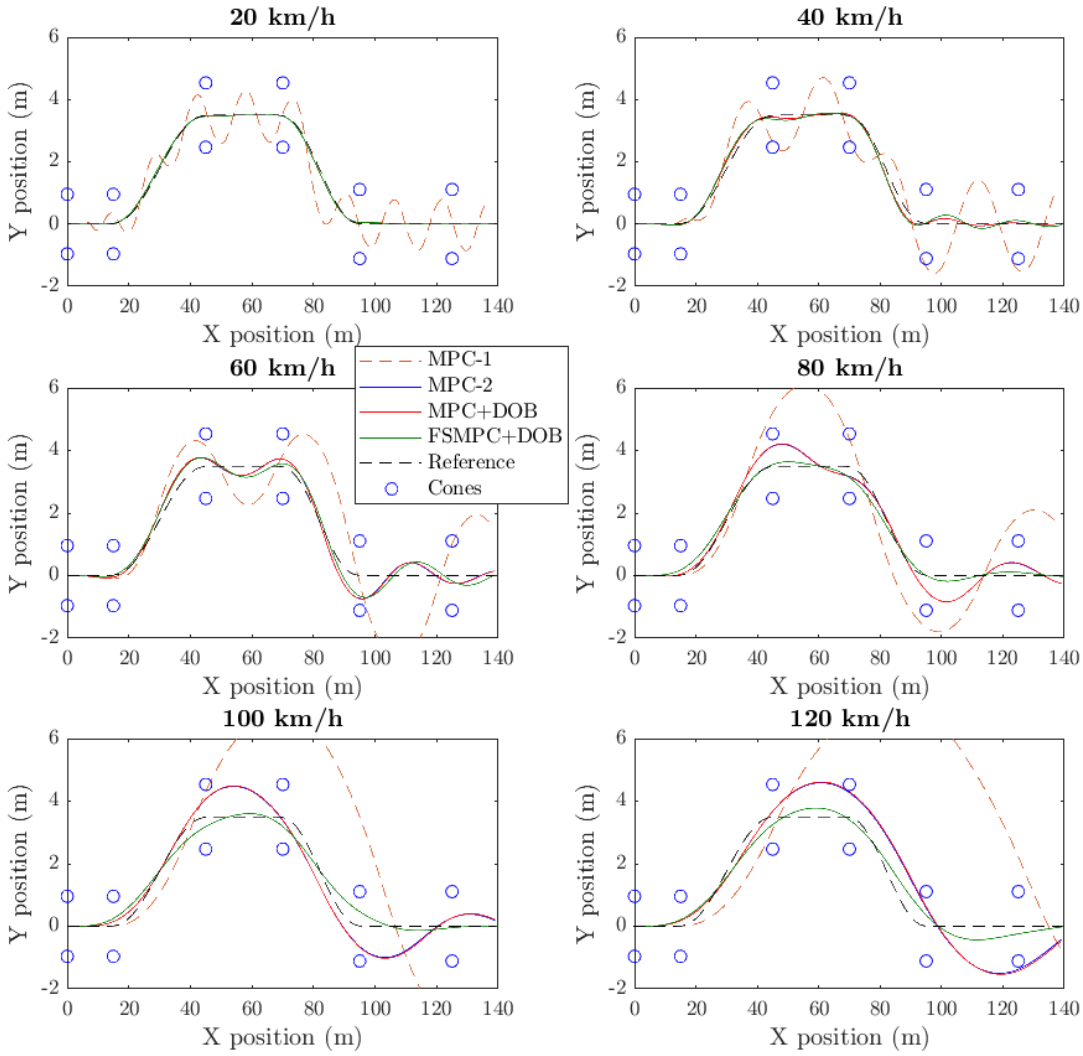

Figure 5-15: Controller tracking performance for double lane change at forward speed of 20 - 120 km/h.

5-3-3 Sinusoidal trajectory

The sinusoidal trajectory designed in Section 5-2 provokes motion sickness by its pre-defined acceleration frequency around 0.2 Hz. Besides, when the vehicle tries to follow the given trajectory at the forward velocity of 60 km/h, the lateral acceleration can exceed 4 m/s^2, where the tire behaviour is nonlinear. Hence, the effect of disturbance rejection and the effect of comfort weighting Q_a are investigated at this scenario, where both the tire nonlinearity and motion discomfort occur.

Effect of Disturbance observer From the previous results on disturbance rejection and double lane change where the tracking performance between MPC-2 and MPC+DOB are almost consistent, it seems that the disturbance observer does not have obvious effect on the mismatch correction. It is because the disturbance observer only corrects the mismatch in output.

Recall the the prediction model described by (3-9) and (3-10), it if found that the output yaw angle is directly computed from state ψ in the prediction state. The output Y is calculated from the T_s based discretization on $\dot{Y}$ that is described by (3-8). Hence, the lateral position Y is related to the prediction to v, ψ, and constant forward velocity u. As indicated in Figure 5-16, the predicted lateral position is largely dependent on u and ψ during such cornering, where the fluctuation of v does not have much influence on $\dot{Y}$. Thus, in our controller where u is fixed at 60 km/h while the prediction model already has a precise prediction on ψ (Figure 5-16), the state error of v that comes from the unmodelled tire nonlinearity only slightly affects the output error of Y, especially when most of our simulations are conducted on the dry asphalt road surface where $\mu = 1$.

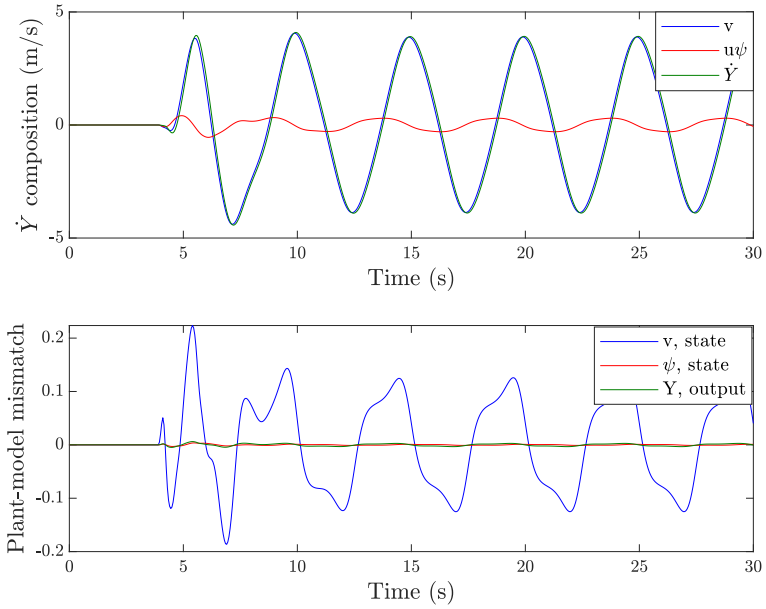

Figure 5-16: Composition of lateral position $\dot{Y}$, plant-model mismatch on tracking signals of MPC-2 at sinusoidal trajectory.

Nonetheless, the disturbance observer works well to correct the acceleration mismatch between plant and prediction model, which is significant for the filtered acceleration based comfort optimization (Figure 5-17). Taking advantages of the acceleration correction and its potential effect on tracking signal correction when cornering on lower friction surface ($\mu \leqslant 1$), the disturbance observer is kept in the proposed solution.

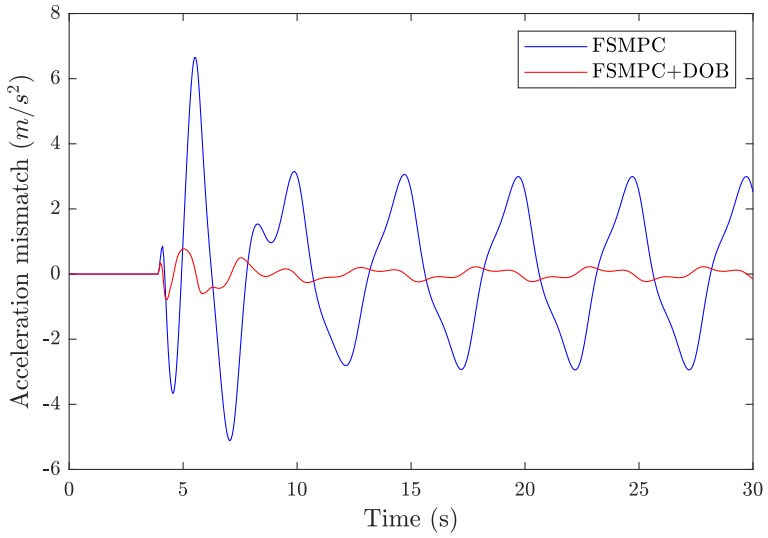

Figure 5-17: Acceleration mismatch between vehicle plant model and MPC model prediction at sinusoidal trajectory.

Effect of comfort weighting Q_a is the weight to optimize driving comfort. As the real trajectory shows in Figure 5-18, the controller that does not take comfort into account (MPC+DOB) tries to follow the planned trajectory as precise as possible. When a penalty is given to the filtered acceleration, the controller starts to make trade-offs between tracking and comfort. Instead of following the exact planned path, the vehicle drives a relatively smoother trajectory by cutting the corners. It is found that the higher the Q_a is, the smoother the trajectory. Such smooth trajectory also helps reduce the magnitude of acceleration due to less displacement. Besides, the power spectrum density (PSD) plot of vehicle acceleration at different Q_a weightings indicates that the FSMPC controller optimizes acceleration with respect to its frequency. Although the peak of acceleration is found at around 0.25 Hz for all Q_a weightings, the controllers with comfort weighting have a lower frequency peak at around 0.25 Hz than the controller without Q_a weighting, whilst they tend to show a second peak at around 0.6 Hz which has lower weightings for both motion sickness and general discomfort according to Figure 2-1. Also, the $W_{f,\text{lateral}}$ and W_d filtered accelerations at around 5 seconds indicate that the FSMPC controller is capable to reduce the passenger perceived sudden shock, where in this scenario such sudden shock comes from the non-smooth curvature between the entry and sinusoidal manoeuvre.

As the tracking and comfort summary indicates in Table 5-7, the growth of Q_a weighting

reduces the values of $a_{y,\mathrm{ms}}$ and $a_{y,\mathrm{ws}}$, the vehicle followed trajectory is therefore more comfortable. On the other hand, when the planned trajectory itself is not comfortable, the tracking error largely increases as Q_a raises, which is even possible to reach a unreasonable level. Therefore the Q_a is supposed to be properly tuned.

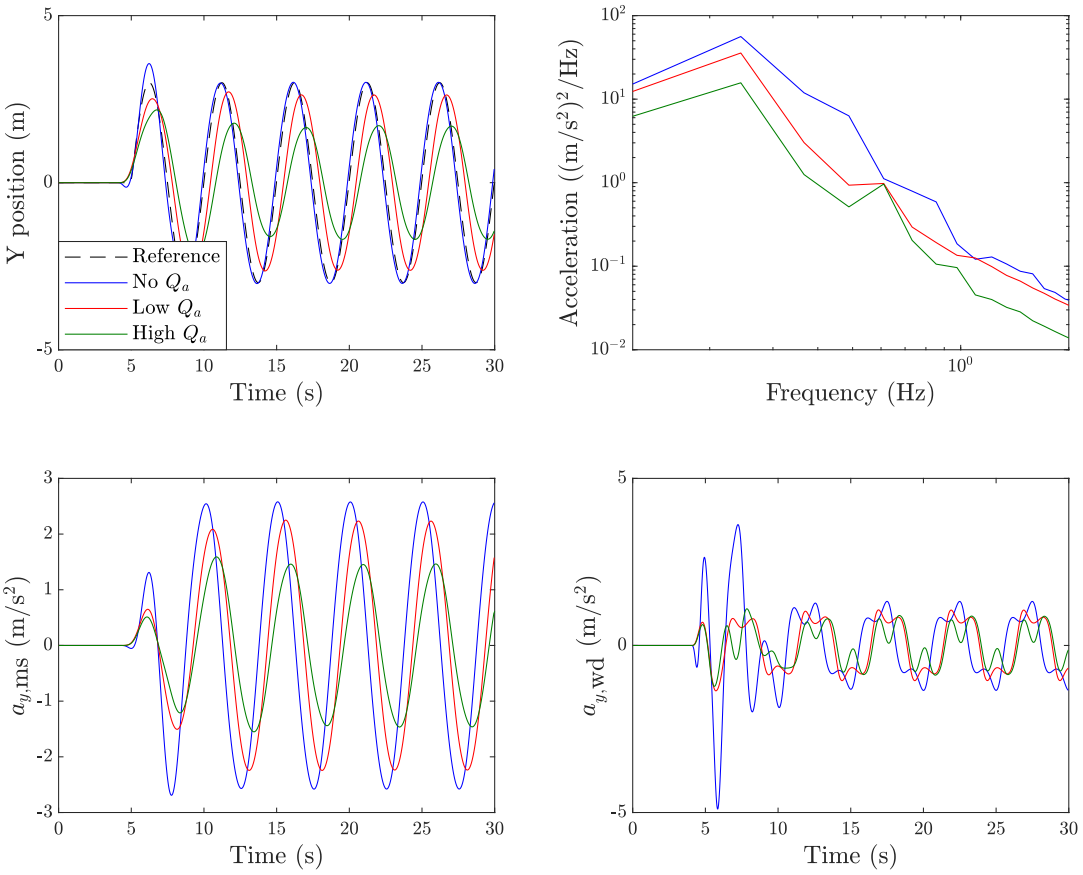

Figure 5-18: Tracking performance, acceleration PSD, $W_{f,\mathrm{lateral}}$ and W_d filtered acceleration histories for sinusoidal trajectory at forward speed 60 km/h.

Table 5-7: Tracking and comfort summary for sinusoidal trajectory at forward speed 60 km/h.

Comfort weighting	Lateral error, peak to peak (m)	Lateral error, mean (m)	$a_{y,\mathrm{ms}}$ (m/s^2)	$a_{y,\mathrm{wd}}$, (m/s^2)
No Q_a	1.1074	0.0035	1.6191	1.1774
Low Q_a	3.5387	0.0231	1.3486	0.6912
High Q_a	5.1900	0.0524	0.9077	0.5309

5-3-4 Summary

From the simulation results of disturbance rejection, it is found that with our tuning, the MPC controller without control effort penalty (MPC-1) is not stable and therefore not comfortable. Compared to this unstable controller, the MPC controllers that includes control effort penalty (MPC-2 and MPC+DOB) improve comfort to a large extent. Based on the MPC+DOB controller, extending the cost function with comfort optimization (FSMPC+DOB) further improves the vehicle motion comfort, where such improvement is based on the comfort assessment criteria. Besides, the comfort improvement is significantly found at the velocity higher than 60 km/h, while the comfort optimization is limited by the controller response to the step crosswind at low forward speed. Also, the simulation on double lane change test ensures that such comfort oriented MPC controller does not cause safety issue.

In the simulation at sinusoidal trajectory, we highlight the effect of disturbance observer on correcting the acceleration prediction, and the effect of comfort weighting Q_a on making trade-offs between tracking accuracy and passenger comfort. Hence, the comfort tuning should be properly chosen.

Chapter 6

Conclusions and future work

6-1 Conclusions

Although the path planning module in automated driving system already improve the passenger comfort by velocity profiles which limits the vehicle acceleration and jerk, the steer input computed by path following controller can still cause uncomfortable motion, especially in the disturbance environment. As the passenger discomfort in a car is introduced by the large acceleration magnitude together with the human-sensitive frequency range, a path following controller that optimizes acceleration with respect to its corresponding frequency is proposed in this study. Taking the frequency shaped cost function that is able to optimize the acceleration frequency, a frequency shaped model predictive controller with linear prediction model is developed. According to ISO 2631, the controller penalizes 0.03 - 0.2 Hz for motion sickness and 1 - 2 Hz for general discomfort. Such penalty is accomplished by adding two bandpass filters on the lateral acceleration and augment the prediction model with two new outputs which represent the filtered accelerations for motion sickness and general discomfort respectively.

As minimizing the acceleration can possibly degrade the steer response, the well-tuned controller is tested in the simulation in three scenarios. As the result presented in Section 5-3, in the simulation of disturbance rejection, for the low speed range 20 - 60 km/h, the FSMPC controller does not improve comfort significantly due to the limitation from the controller response to crosswind, while at the high speed range 80 - 120 km/h, the FSMPC controller can improve the motion sickness index $a_{y,\mathrm{ms}}$ up to 40% and the general discomfort index $a_{y,\mathrm{wd}}$ up to 50%, compared to the stable MPC-2 and MPC+DOB controllers. In the meantime, the tracking errors for all tests are kept under 0.1 m, even smaller than the sensor noise of 0.2 m. Meanwhile, the vehicle plant is able to pass the double lane change under the control of FSMPC controller for all the tested velocity, which verifies the emergency handling ability of the FSMOC controller. From the simulations, the FSMPC controller shows its ability of balancing passenger discomfort with handling performance.

Further, as a linear prediction model is used to control the nonlinear vehicle plant, the prediction error always exists. A disturbance observer is applied to the controller, trying to correct

such mismatch. The disturbance observer does not have obvious effect on improving the tracking performance, since the plant-model output mismatch on tracking signals are small in the simulation scenarios. Nonetheless, the disturbance observer is found to be able to correct the acceleration prediction to a large extent. Taking advantages of such acceleration correction, and its potential effect on tracking signal correction during the low friction cornering that is not included in our simulation, the disturbance observer is kept in the proposed solution.

6-2 Future work

6-2-1 Effect of disturbance observer

As discussed in Section 5-3-3, the disturbance observer helps to correct the acceleration prediction to a large extent but do not have much effect on improving the prediction of tracking signals. Further, due to the presence of sensor noise, the disturbance observer gives a wrong feedback to the prediction model and therefore enlarge the plant-model mismatch. On the other hand, due to the high nonlinearity of the vehicle plant, unlike the simulation scenarios in this study, the plant-model mismatch can be large when the vehicle is cornering on the low friction surface, where the disturbance observer should be able to improve the tracking signal prediction to a great extent, from the theoretical point of view. Therefore the simulation of low friction surface cornering should be introduced to test the effect of disturbance observer, before deciding whether the disturbance observer is necessary to be applied on the tracking signals.

6-2-2 Improvement on prediction model

As this study aims at developing a comfort optimization on frequency dependent acceleration in the path following controller, a simple 2-DOF linear dynamic bicycle model is used as the prediction model. Due to the nonlinearity of the tire model and vehicle plant, as well as the unmodelled details between the bicycle model and the 9-DOF vehicle plant, the prediction is not accurate and therefore the compute steer input is not optimal to the vehicle plant. In order the make the prediction model as precise to the vehicle plant as possible, the tire nonlinearity should be taken into account in the prediction model. Therefore instead of the linear bicycle model, the nonlinear bicycle model that adopts Magic Formula to calculate the tire forces should be applied. Or, for the purpose of reducing the computational intensity, the linear time varying (LTV) or linear parameter varying (LPV) bicycle model can be adopted. On the other hand, the prediction error due to unmodelled details can be compensated by a disturbance observer.

6-2-3 Tracking-comfort balancing

As the proposed solution optimizes comfort by regulating the acceleration, the high weights given to comfort can degrade the tracking accuracy. Instead of finding one set of weightings to realize the trade-offs, in order to optimize comfort to the largest extent without affecting the vehicle handling performance, the controller should distinguish between normal following and emergency handling, where the higher penalty can be given to comfort in the normal driving

scenario while the comfort demand can be relax when the fast steer response is required. One way is to do the gain scheduling on comfort weightings regarding the increments of planned heading angle, as in the emergency situations such as evasive manoeuvre, the change rate of heading angle is usually large. Another way to do so is to extend the comfort weighting with path discontinuity defined by the difference between current heading angle and the planned heading angle in the following time steps, then the comfort optimization can be relaxed when the path is discontinued.

6-2-4 Improvement on comfort design

The FSMPC performance at low speed (20 - 60 km/h) is limited by the controller response at the crosswind rejection. The poorly damped oscillation may be able to improve by carefully choosing the comfort filter. In this study the filter is simplified as two bandpass filters according to $W_{f,\text{lateral}}$ and W_d, which are possible to be further improved by adjusting the filter slope, or alternatively, using one proper-designed bandstop filter, according to the actual requirements.

The motion sickness that is taken into account in this study highlights the acceleration has corresponding frequency in the range of 0.03 - 0.2 Hz. Meanwhile, the prediction time we adopt is 1 s. The prediction to $W_{f,\text{lateral}}$ filtered acceleration is therefore not accurate, while using a long prediction time longer than 5 s is not feasible. Although the motion sickness improvement is achieved in our controller design, the following questions still remain: (i) if a longer prediction time can further improve the motion sickness index, (ii) if including the acceleration history from former plant output in the FSMPC optimization can further improve the motion sickness index.

6-2-5 Subjective experiment

This study investigates the passenger comfort improvement on path following controller by minimizing the comfort indices. However comfort as a subjective concept is always not accurate to be evaluated by a number. The most intuitive way to assess the FSMPC controller performance is to conduct a subjective experiment where the participants can rate their comfort feelings as passengers on the car driven by the FSMPC controller.

Appendix A

Controller tuning process

A-1 Controller parameter tuning

The sampling time T_s is chosen to be 0.05 s for a fast controller response to the reference signal. This sampling time is also well-adopted in path following controller design [19–21, 52]. In order to make the comparison, we try to obtain a baseline controller (MPC-2) that is stable in the designed scenarios as many as possible.

As the lateral deviation should be emphasized while the weight on steer input helps to stabilize the controller, the Q matrix for terminal tracking error and R matrix are tuned as follows, so as the coefficient a for the tracking error penalty for the intermediate states.

- $Q = \begin{bmatrix} 1000 & 0 \\ 0 & 80 \end{bmatrix}$,
- $R = 500$,
- $a =$ 1E-6.

where Q_{11} is the weight for lateral error, Q_{22} is the weight for yaw error, R is the weight for increments of steering angle.

In order to find the optimal prediction horizon N_p that can stabilize the vehicle plant at even the high velocity with disturbances, the simulation with various N_p is conducted at combined disturbances rejection as described in Scenario 1, Case 3 at forward speed of 120 km/h. The N_p tested in the tuning process is in the range of 3 - 200, corresponding to the prediction time from 0.15 s to 10 s. The simulation result is plotted as in Figure A-1. Also, as we emphasize the output of terminal state and the smooth steer control, a proper prediction horizon should be selected to preserve the transient behaviour in the intermediate states. The simulation on various N_p is therefore conducted on scenario 3 as plotted in Figure A-2. Taking the total costs and tracking errors for both scenarios into account, the optimal prediction time is found at 1 s, corresponding to $N_p = 20$. Also, the real-time implementation is a critical concern

for MPC controller. Although the computational time increases as the increase of prediction horizon, it is found that the prediction horizon we choose satisfies the requirement.

Further, as the common comfort penalty that works for all given velocities is not found, a gain scheduling is applied on Q_a.

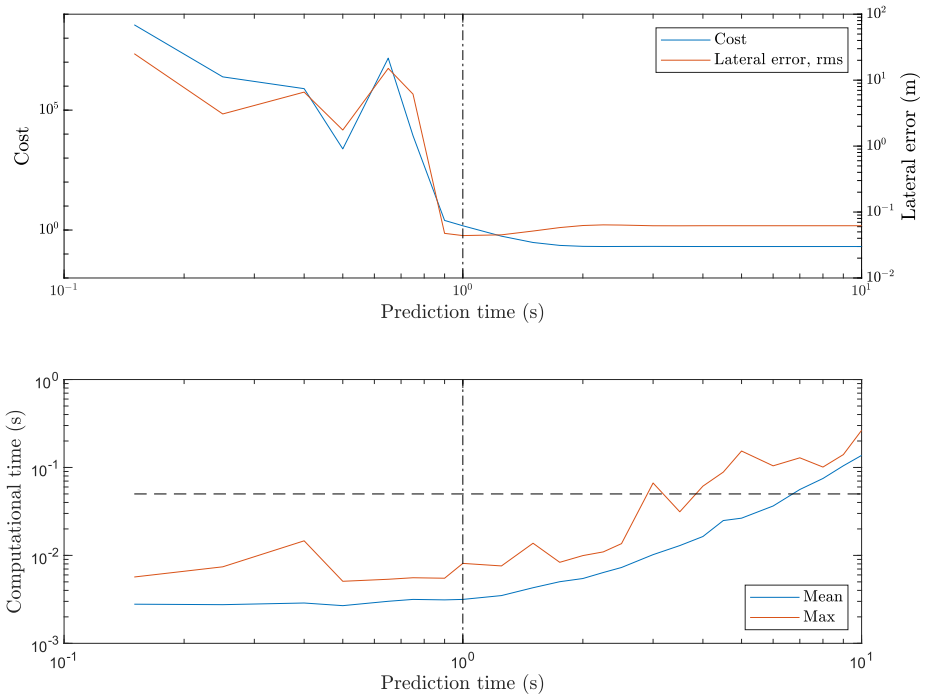

Figure A-1: Controller cost and lateral error for various prediction time, controller computational time at combined disturbances rejection with forward speed of 120 km/h. The horizontal dash line indicates the real-time threshold, the vertical dash-dot line indicates the chosen prediction time.

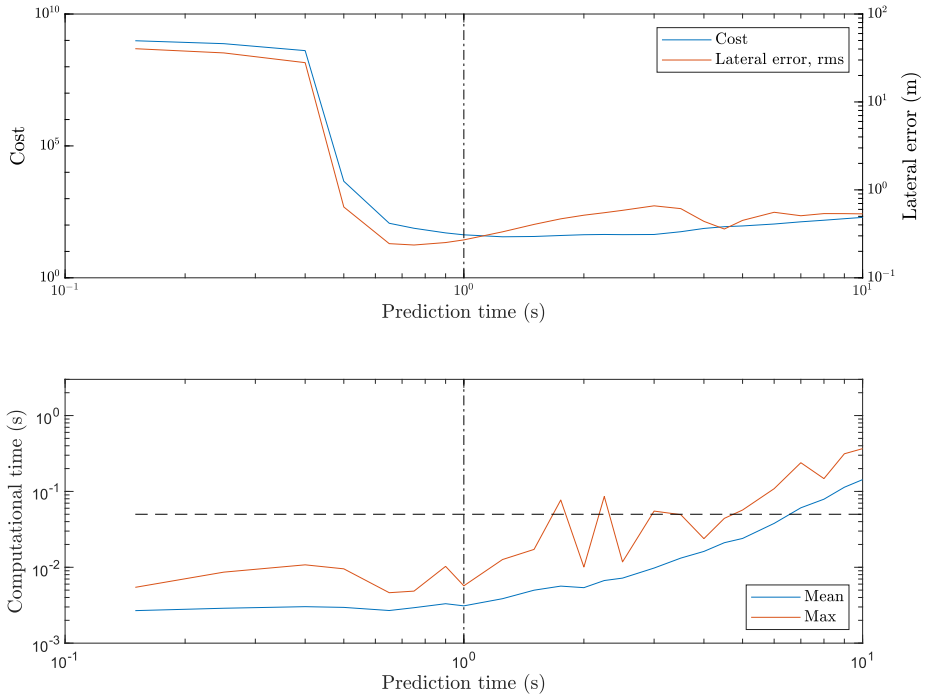

Figure A-2: Controller cost and lateral error for various prediction time, controller computational time at sinusoidal trajectory.The horizontal dash line indicates the real-time threshold, the vertical dash-dot line indicates the chosen prediction time.

A-2 Discussion on long prediction horizon

Motion sickness is one of the concepts of passenger comfort that we highlight in this study, which requires to reject the acceleration from 0.03 to 0.2 Hz. Meanwhile, as we adopt the prediction time of 1 s ($N_p = 20$), the optimization of $a_{y,\mathrm{ms}}$ in the controller is not accurate. Taking prediction time of 10 s ($N_p = 200$) as example, the effect of long prediction horizon on improving motion sickness in FSMPC controller is investigated.

As mentioned in last section, as our control strategy emphasizes the tracking accuracy of the terminal output and the smoothness of steer input, the transient behaviour is lost when the prediction horizon is increased, so the tracking error is unreasonably large. Firstly, the coefficient a is re-tuned to 1E-4 to obtain a reasonable tracking performance to the sinusoidal trajectory (scenario 3) as indicated in Figure A-3.

Compare the comfort indices of $N_p = 200$ to $N_p = 20$, no improvement is found regarding both motion sickness and general discomfort at both scenarios (Table A-1), the prediction horizon is therefore kept to be 20, corresponding to prediction time of 1 s.

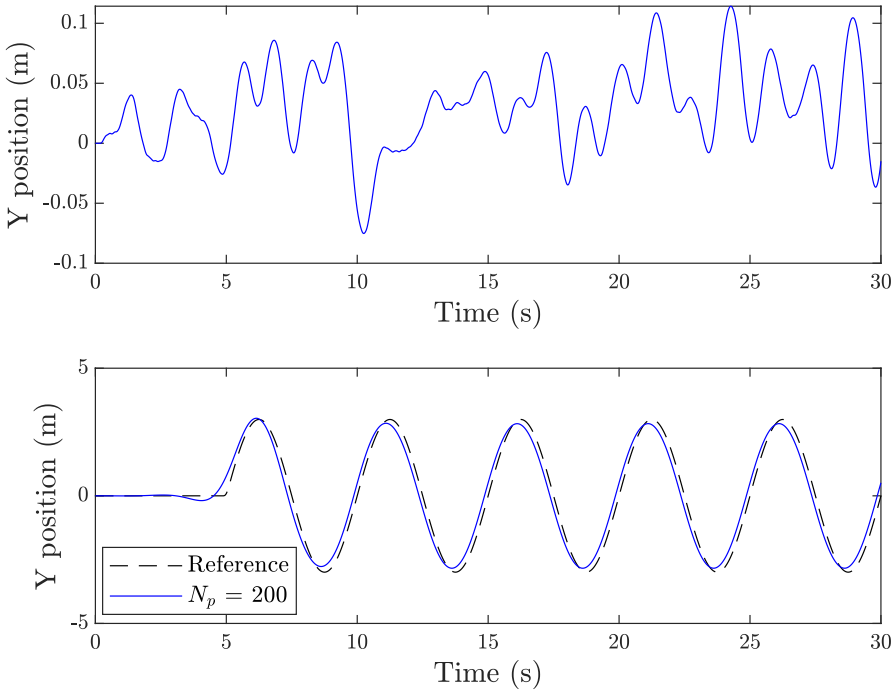

Figure A-3: Tracking performance of FSMPC controller with $N_p = 200$, at scenario 1, case 3 at 120 km/h, and scenario 3 at 60 km/h.

Table A-1: Comfort performance of FSMPC controller with $N_p = 20$ and $N_p = 200$.

Scenario	N_p	$a_{y,\mathrm{ms}}$	$a_{y,\mathrm{wd}}$
Scenario 1, case 3	20	0.0215	0.2032
	200	0.0294	0.3317
Scenario 3	20	1.3486	0.6912
	200	1.5036	0.8047

Appendix B

State-space matrices of prediction model

B-1 Continuous-time bicycle model in prediction model

20 km/h:

$$A = \begin{bmatrix} -53.9228 & 13.6651 & 0 & 0 \\ 10.7989 & -58.5558 & 0 & 0 \\ 1.0000 & 0 & 0 & 5.5556 \\ 0 & 1.0000 & 0 & 0 \end{bmatrix} \quad B = \begin{bmatrix} 135.4232 \\ 85.4444 \\ 0 \\ 0 \end{bmatrix}$$

$$C = \begin{bmatrix} 0 & 0 & 1.0000 & 0 \\ 0 & 0 & 0 & 1.0000 \\ -53.9228 & 19.2206 & 0 & 0 \end{bmatrix} \quad D = \begin{bmatrix} 0 \\ 0 \\ 135.4232 \end{bmatrix}$$

40 km/h:

$$A = \begin{bmatrix} -26.9614 & -1.5008 & 0 & 0 \\ 5.3994 & -29.2779 & 0 & 0 \\ 1.0000 & 0 & 0 & 11.1111 \\ 0 & 1.0000 & 0 & 0 \end{bmatrix} \quad B = \begin{bmatrix} 135.4232 \\ 85.4444 \\ 0 \\ 0 \end{bmatrix}$$

$$C = \begin{bmatrix} 0 & 0 & 1.0000 & 0 \\ 0 & 0 & 0 & 1.0000 \\ -26.9614 & 9.6103 & 0 & 0 \end{bmatrix} \quad D = \begin{bmatrix} 0 \\ 0 \\ 135.4232 \end{bmatrix}$$

60 km/h:

$$A = \begin{bmatrix} -17.9743 & -10.2598 & 0 & 0 \\ 3.5996 & -19.5186 & 0 & 0 \\ 1.0000 & 0 & 0 & 16.6667 \\ 0 & 1.0000 & 0 & 0 \end{bmatrix} \quad B = \begin{bmatrix} 135.4232 \\ 85.4444 \\ 0 \\ 0 \end{bmatrix}$$

$$C = \begin{bmatrix} 0 & 0 & 1.0000 & 0 \\ 0 & 0 & 0 & 1.0000 \\ -17.9743 & 6.4069 & 0 & 0 \end{bmatrix} \quad D = \begin{bmatrix} 0 \\ 0 \\ 135.4232 \end{bmatrix}$$

80 km/h:

$$A = \begin{bmatrix} -13.4807 & -17.4171 & 0 & 0 \\ 2.6997 & -14.6389 & 0 & 0 \\ 1.0000 & 0 & 0 & 22.2222 \\ 0 & 1.0000 & 0 & 0 \end{bmatrix} \quad B = \begin{bmatrix} 135.4232 \\ 85.4444 \\ 0 \\ 0 \end{bmatrix}$$

$$C = \begin{bmatrix} 0 & 0 & 1.0000 & 0 \\ 0 & 0 & 0 & 1.0000 \\ -13.4807 & 4.8052 & 0 & 0 \end{bmatrix} \quad D = \begin{bmatrix} 0 \\ 0 \\ 135.4232 \end{bmatrix}$$

100 km/h:

$$A = \begin{bmatrix} -10.7846 & -23.9337 & 0 & 0 \\ 2.1598 & -11.7112 & 0 & 0 \\ 1.0000 & 0 & 0 & 27.7778 \\ 0 & 1.0000 & 0 & 0 \end{bmatrix} \quad B = \begin{bmatrix} 135.4232 \\ 85.4444 \\ 0 \\ 0 \end{bmatrix}$$

$$C = \begin{bmatrix} 0 & 0 & 1.0000 & 0 \\ 0 & 0 & 0 & 1.0000 \\ -10.7846 & 3.8441 & 0 & 0 \end{bmatrix} \quad D = \begin{bmatrix} 0 \\ 0 \\ 135.4232 \end{bmatrix}$$

120 km/h:

$$A = \begin{bmatrix} -8.9871 & -30.1299 & 0 & 0 \\ 1.7998 & -9.7593 & 0 & 0 \\ 1.0000 & 0 & 0 & 33.3333 \\ 0 & 1.0000 & 0 & 0 \end{bmatrix} \quad B = \begin{bmatrix} 135.4232 \\ 85.4444 \\ 0 \\ 0 \end{bmatrix}$$

$$C = \begin{bmatrix} 0 & 0 & 1.0000 & 0 \\ 0 & 0 & 0 & 1.0000 \\ -8.9871 & 3.2034 & 0 & 0 \end{bmatrix} \quad D = \begin{bmatrix} 0 \\ 0 \\ 135.4232 \end{bmatrix}$$

B-2 Comfort filter and corresponding discrete filter in prediction model

Comfort filter:

$$\text{Motion sickness filter} \qquad F_{\text{ms}}(\omega) = \frac{1.257\omega}{\omega^2 + 1.445\omega + 0.2369}$$

$$\text{General discomfort filter} \qquad F_{\text{wd}}(\omega) = \frac{12.57\omega}{\omega^2 + 18.85\omega + 78.96}$$

Comfort filter in discrete-time state space:

$$A_f = \begin{bmatrix} 0.9300 & -0.0114 & 0 & 0 \\ 0.0482 & 0.9997 & 0 & 0 \\ 0 & 0 & 0.3366 & -2.4745 \\ 0 & 0 & 0.0313 & 0.9273 \end{bmatrix} \quad B_f = \begin{bmatrix} 0.0482 \\ 0.0012 \\ 0.0313 \\ 0.0009 \end{bmatrix}$$

$$C_f = \begin{bmatrix} 1.2566 & 0 & 0 & 0 \\ 0 & 0 & 12.5664 & 0 \end{bmatrix} \qquad D_f = \begin{bmatrix} 0 \\ 0 \end{bmatrix}$$

Appendix C

Controller performance summary for disturbance rejection

Table C-1: Controller performance summary for disturbance rejection of crosswind.

Forward Speed (km/h)	Controller	Lateral error (m)			Motion sickness		General discomfort	
		Peak to peak	Mean	R.M.S	$a_{y,\mathrm{ms}}$ (m/s^2)	Improvement	$a_{y,wd}$ (m/s^2)	Improvement
20	No control	1.5525	0.5336	0.7057	0.0007	15.01%	0.0055	6.67%
	MPC-1	1.6447	-0.0216	0.5320	0.6613	99.90%	1.7226	99.66%
	MPC-2	0.0059	0.0049	0.0050	0.0006	(6.26%)	0.0060	2.71%
	MPC+DOB	0.0058	0.0048	0.0049	0.0006	(8.85%)	0.0061	3.94%
	FSMPC+DOB	0.0063	0.0052	0.0053	0.0006	−−	0.0059	−−
40	No control	5.5603	1.8486	2.4836	0.0022	34.26%	0.0050	(37.06%)
	MPC-1	2.7016	0.0037	0.8818	1.0824	99.87%	3.6319	99.78%
	MPC-2	0.0107	0.0088	0.0090	0.0010	(30.87%)	0.0070	(11.92%)
	MPC+DOB	0.0105	0.0086	0.0088	0.0010	(32.21%)	0.0070	(11.97%)
	FSMPC+DOB	0.0151	0.0127	0.0130	0.0015	−−	0.0080	−−
60	No control	11.4502	3.7564	5.0792	0.0044	28.79%	0.0050	(69.56%)
	MPC-1	2.8623	0.0441	0.9565	1.1571	99.73%	4.4581	99.63%
	MPC-2	0.0158	0.0129	0.0132	0.0014	(54.55%)	0.0094	(43.28%)
	MPC+DOB	0.0155	0.0126	0.0129	0.0014	(55.15%)	0.0093	(43.50%)
	FSMPC+DOB	0.0322	0.0250	0.0257	0.0031	−−	0.0165	−−
80	No control	18.4981	6.0236	8.1741	0.0071	38.59%	0.0052	(68.61%)
	MPC-1	4.2267	0.0405	1.0687	1.2690	99.66%	4.5096	99.63%
	MPC-2	0.0208	0.0168	0.0172	0.0019	(57.16%)	0.0121	(26.90%)
	MPC+DOB	0.0205	0.0165	0.0169	0.0018	(57.51%)	0.0121	(26.84%)
	FSMPC+DOB	0.0500	0.0441	0.0452	0.0043	−−	0.0166	−−
100	No control	26.0189	8.4327	11.4694	0.0099	54.12%	0.0055	(64.40%)
	MPC-1	1.8974	0.0456	0.5853	0.5947	99.24%	5.2422	99.71%
	MPC-2	0.0255	0.0204	0.0209	0.0023	(49.88%)	0.0151	(1.50%)
	MPC+DOB	0.0252	0.0201	0.0205	0.0023	(50.08%)	0.0152	(0.74%)
	FSMPC+DOB	0.0539	0.0504	0.0517	0.0045	−−	0.0154	−−
120	No control	33.4794	10.8160	14.7338	0.0127	74.68%	0.0058	(57.25%)
	MPC-1	19.1751	-8.0013	10.2766	0.7606	99.58%	20.1407	99.93%
	MPC-2	0.0297	0.0237	0.0242	0.0027	(16.77%)	0.0184	26.82%
	MPC+DOB	0.0294	0.0232	0.0238	0.0027	(16.70%)	0.0187	27.94%
	FSMPC+DOB	0.0372	0.0331	0.0339	0.0032	−−	0.0135	−−

* The improvement indicates the improvement on comfort index of the FSMPC controller compared to the corresponding controller. (·) indicates the corresponding baseline controller has smaller comfort index, the improvement is found in reverse.

Table C-2: Controller performance summary for disturbance rejection of sensor noise.

Forward Speed (km/h)	Controller	Lateral error (m)			Motion sickness		General discomfort	
		Peak to peak	Mean	R.M.S	$a_{y,\text{ms}}$ (m/s^2)	Improvement	$a_{y,wd}$ (m/s^2)	Improvement
20	MPC-1	5.4414	-0.1799	1.1322	1.0894	97.82%	1.4220	86.78%
	MPC-2	0.1432	0.0030	0.0257	0.0226	(4.75%)	0.1752	(6.80%)
	MPC+DOB	0.1452	0.0031	0.0259	0.0226	(4.93%)	0.1946	3.42%
	FSMPC+DOB	0.1482	0.0031	0.0265	0.0237	−−	0.1880	−−
40	MPC-1	3.3667	-0.0928	1.0733	1.3268	97.66%	3.5688	93.37%
	MPC-2	0.1575	0.0029	0.0297	0.0266	(14.36%)	0.2399	1.32%
	MPC+DOB	0.1606	0.0030	0.0301	0.0269	(13.33%)	0.2536	6.65%
	FSMPC+DOB	0.1738	0.0031	0.0325	0.0311	−−	0.2367	−−
60	MPC-1	3.5012	-0.0387	1.1283	1.3890	97.73%	4.3723	94.36%
	MPC-2	0.1550	0.0027	0.0321	0.0280	(11.10%)	0.2954	16.48%
	MPC+DOB	0.1584	0.0028	0.0327	0.0286	(9.25%)	0.3069	19.61%
	FSMPC+DOB	0.1635	0.0031	0.0332	0.0315	−−	0.2467	−−
80	MPC-1	6.5146	-0.0453	1.8812	2.2145	99.01%	3.7656	95.17%
	MPC-2	0.1613	0.0025	0.0341	0.0291	24.86%	0.3326	45.27%
	MPC+DOB	0.1636	0.0026	0.0348	0.0298	26.71%	0.3433	46.97%
	FSMPC+DOB	0.1395	0.0028	0.0257	0.0219	−−	0.1821	−−
100	MPC-1	34.8152	-3.6878	10.2476	0.8317	97.76%	9.7649	98.12%
	MPC-2	0.1727	0.0024	0.0359	0.0303	38.45%	0.3602	49.14%
	MPC+DOB	0.1756	0.0025	0.0367	0.0311	40.09%	0.3701	50.50%
	FSMPC+DOB	0.1298	0.0026	0.0237	0.0186	−−	0.1832	−−
120	MPC-1	66.3099	-27.5108	35.7357	0.6024	96.35%	28.7746	99.13%
	MPC-2	0.1959	0.0024	0.0376	0.0315	30.06%	0.3818	34.48%
	MPC+DOB	0.2007	0.0025	0.0385	0.0323	31.96%	0.3905	35.94%
	FSMPC+DOB	0.1432	0.0025	0.0269	0.0220	−−	0.2501	−−

* The improvement indicates the improvement on comfort index of the FSMPC controller compared to the corresponding controller. (·) indicates the corresponding baseline controller has smaller comfort index, the improvement is found in reverse.

Table C-3: Controller performance summary for disturbance rejection of combined disturbances.

Forward Speed (km/h)	Controller	Lateral error (m)			Motion sickness		General discomfort	
		Peak to peak	Mean	R.M.S	$a_{y,\text{ms}}$ (m/s^2)	Improvement	$a_{y,wd}$ (m/s^2)	Improvement
20	MPC-1	4.0507	0.7168	1.3300	0.2490	90.11%	0.2505	29.55%
	MPC-2	0.1434	0.0094	0.0274	0.0231	(6.25%)	0.1686	(4.45%)
	MPC+DOB	0.1460	0.0100	0.0280	0.0234	(5.01%)	0.1828	3.45%
	FSMPC+DOB	0.1486	0.0106	0.0288	0.0246	−−	0.1765	−−
40	MPC-1	17.2836	5.0972	8.1058	0.1489	78.89%	0.3783	47.72%
	MPC-2	0.1613	0.0137	0.0324	0.0269	(14.34%)	0.2104	5.98%
	MPC+DOB	0.1653	0.0146	0.0332	0.0276	(12.10%)	0.2147	7.86%
	FSMPC+DOB	0.1768	0.0192	0.0374	0.0314	−−	0.1978	−−
60	MPC-1	30.4717	16.2986	19.5286	0.1417	79.57%	0.6041	68.95%
	MPC-2	0.1591	0.0181	0.0355	0.0272	(5.99%)	0.2365	20.69%
	MPC+DOB	0.1636	0.0190	0.0363	0.0280	(3.31%)	0.2348	20.11%
	FSMPC+DOB	0.1669	0.0322	0.0446	0.0289	−−	0.1875	−−
80	MPC-1	38.4355	12.2478	17.5031	0.1382	84.60%	0.9327	83.73%
	MPC-2	0.1580	0.0220	0.0383	0.0274	22.24%	0.2480	38.83%
	MPC+DOB	0.1630	0.0229	0.0391	0.0282	24.43%	0.2446	37.96%
	FSMPC+DOB	0.1398	0.0514	0.0582	0.0213	−−	0.1517	−−
100	MPC-1	23.2479	14.0409	15.8176	0.1952	90.64%	1.0198	84.57%
	MPC-2	0.1563	0.0256	0.0411	0.0278	34.18%	0.2560	38.54%
	MPC+DOB	0.1624	0.0264	0.0419	0.0286	36.06%	0.2524	37.67%
	FSMPC+DOB	0.1280	0.0581	0.0639	0.0183	−−	0.1573	−−
120	MPC-1	43.4780	21.1067	25.1350	0.2703	92.04%	1.0244	80.16%
	MPC-2	0.1606	0.0288	0.0440	0.0285	24.45%	0.2636	22.91%
	MPC+DOB	0.1660	0.0295	0.0447	0.0293	26.63%	0.2606	22.04%
	FSMPC+DOB	0.1432	0.0388	0.0474	0.0215	−−	0.2032	−−

* The improvement indicates the improvement on comfort index of the FSMPC controller compared to the corresponding controller. (·) indicates the corresponding baseline controller has smaller comfort index, the improvement is found in reverse.

Appendix D

List of optimal cost for each component at disturbance rejection

Table D-1: Controller cost for disturbance rejection of crosswind.

Forward Speed (km/h)	Controller	J_{tracking}	$J_{\Delta u}$	J_{ms}	J_{wd}	J
20	MPC-1	1.057E+04	(0)	(0)	(0)	1.057E+04
	MPC-2	0.034	0.006	(0)	(0)	0.039
	MPC+DOB	0.033	0.006	(0)	(0)	0.039
	FSMPC+DOB	0.043	0.006	0.014	0.059	0.123
40	MPC-1	633.421	(0)	(0)	(0)	633.421
	MPC-2	0.012	0.010	(0)	(0)	0.022
	MPC+DOB	0.012	0.010	(0)	(0)	0.022
	FSMPC+DOB	0.064	0.016	0.393	0.287	0.760
60	MPC-1	6.664	(0)	(0)	(0)	6.664
	MPC-2	0.006	0.010	(0)	(0)	0.016
	MPC+DOB	0.006	0.010	(0)	(0)	0.016
	FSMPC+DOB	0.112	0.057	0.244	1.207	1.620
80	MPC-1	4.247	(0)	(0)	(0)	4.247
	MPC-2	0.004	0.010	(0)	(0)	0.014
	MPC+DOB	0.004	0.010	(0)	(0)	0.014
	FSMPC+DOB	0.354	0.080	0.738	2.361	3.533
100	MPC-1	0.899	(0)	(0)	(0)	0.899
	MPC-2	0.004	0.009	(0)	(0)	0.013
	MPC+DOB	0.004	0.009	(0)	(0)	0.013
	FSMPC+DOB	0.336	0.061	0.753	2.401	3.551
120	MPC-1	7.447E+10	(0)	(0)	(0)	7.447E+10
	MPC-2	0.004	0.009	(0)	(0)	0.013
	MPC+DOB	0.004	0.009	(0)	(0)	0.013
	FSMPC+DOB	0.038	0.014	0.180	0.669	0.900
120 ($N_p = 200$)	MPC-1	1.423E+12	(0)	(0)	(0)	1.423E+12
	MPC-2	0.022	0.003	(0)	(0)	0.025
	MPC+DOB	0.022	0.003	(0)	(0)	0.025
	FSMPC+DOB	0.015	0.013	2.794	0.668	3.490

* (0) indicates the corresponding term of cost is not included in the cost function.
** The responses to MPC-1 are unstable.

Table D-2: Controller cost for disturbance rejection of sensor noise.

Forward Speed (km/h)	Controller	J_{tracking}	$J_{\Delta u}$	J_{ms}	J_{wd}	J
20	MPC-1	4.426E+05	(0)	(0)	(0)	4.426E+05
	MPC-2	39.924	17.984	(0)	(0)	57.908
	MPC+DOB	195.604	87.936	(0)	(0)	283.541
	FSMPC+DOB	196.164	87.578	0.732	4.572	289.046
40	MPC-1	2.149E+03	(0)	(0)	(0)	2.149E+03
	MPC-2	9.507	7.747	(0)	(0)	17.254
	MPC+DOB	45.704	35.872	(0)	(0)	81.576
	FSMPC+DOB	48.543	33.493	6.968	8.414	97.418
60	MPC-1	46.292	(0)	(0)	(0)	46.292
	MPC-2	2.859	4.545	(0)	(0)	7.403
	MPC+DOB	13.379	20.325	(0)	(0)	33.704
	FSMPC+DOB	23.795	13.038	2.238	16.345	55.415
80	MPC-1	21	(0)	(0)	(0)	21
	MPC-2	1.154	2.782	(0)	(0)	3.936
	MPC+DOB	5.277	12.102	(0)	(0)	17.379
	FSMPC+DOB	18.218	6.275	5.109	18.439	48.041
100	MPC-1	3.763E+10	(0)	(0)	(0)	3.763E+10
	MPC-2	0.599	1.836	(0)	(0)	2.436
	MPC+DOB	2.690	7.807	(0)	(0)	10.497
	FSMPC+DOB	13.182	4.450	4.539	15.139	37.311
120	MPC-1	3.989E+11	(0)	(0)	(0)	3.989E+11
	MPC-2	0.376	1.300	(0)	(0)	1.677
	MPC+DOB	1.665	5.424	(0)	(0)	7.089
	FSMPC+DOB	5.709	3.505	0.811	5.549	15.575
120 ($N_p = 200$)	MPC1	1.634E+13	(0)	(0)	(0)	1.634E+13
	MPC2	0.149	0.035	(0)	(0)	0.184
	MPC+DOB	0.712	0.158	(0)	(0)	0.870
	FSMPC+DOB	0.926	0.064	0.121	0.152	1.262

* (0) indicates the corresponding term of cost is not included in the cost function.
** The responses to MPC-1 are unstable.

Table D-3: Controller cost for disturbance rejection of combined disturbances.

Forward Speed (km/h)	Controller	J_{tracking}	$J_{\Delta u}$	J_{ms}	J_{wd}	J
20	MPC-1	3.790E+03	(0)	(0)	(0)	3.790E+03
	MPC-2	39.959	17.942	(0)	(0)	57.901
	MPC+DOB	195.620	87.847	(0)	(0)	283.468
	FSMPC+DOB	196.213	87.483	0.753	4.563	289.011
40	MPC-1	1.604E+05	(0)	(0)	(0)	1.604E+05
	MPC-2	9.373	7.599	(0)	(0)	16.972
	MPC+DOB	45.530	35.671	(0)	(0)	81.202
	FSMPC+DOB	48.362	33.217	7.265	8.210	97.053
60	MPC-1	7.788E+06	(0)	(0)	(0)	7.788E+06
	MPC-2	2.750	4.322	(0)	(0)	7.072
	MPC+DOB	13.246	20.049	(0)	(0)	33.295
	FSMPC+DOB	23.723	12.876	2.448	17.095	56.142
80	MPC-1	1.396E+06	(0)	(0)	(0)	1.396E+06
	MPC-2	1.087	2.572	(0)	(0)	3.659
	MPC+DOB	5.199	11.855	(0)	(0)	17.053
	FSMPC+DOB	18.584	6.336	5.884	21.001	51.804
100	MPC-1	4.197E+04	(0)	(0)	(0)	4.197E+04
	MPC-2	0.557	1.660	(0)	(0)	2.217
	MPC+DOB	2.642	7.607	(0)	(0)	10.249
	FSMPC+DOB	13.571	4.511	5.365	17.940	41.388
120	MPC-1	8.825E+04	(0)	(0)	(0)	8.825E+04
	MPC-2	0.348	1.157	(0)	(0)	1.505
	MPC+DOB	1.634	5.266	(0)	(0)	6.900
	FSMPC+DOB	5.727	3.500	1.015	6.359	16.602
120 ($N_p = 200$)	MPC1	4.420E+3	(0)	(0)	(0)	4.420E+3
	MPC2	0.168	0.037	(0)	(0)	0.205
	MPC+DOB	0.732	0.159	(0)	(0)	0.891
	FSMPC+DOB	0.942	0.077	2.969	0.834	4.822

* (0) indicates the corresponding term of cost is not included in the cost function.
** The responses to MPC-1 are unstable.

Bibliography

[1] B. E. Donohew and M. J. Griffin, "Motion sickness: effect of the frequency of lateral oscillation," *Aviation, Space, and Environmental Medicine*, vol. 75, no. 8, pp. 649–656, 2004.

[2] "Mechanical vibration and shock - Evaluation of human exposure to whole-body vibration - part 1: General requirements," International Organization for Standardization, Standard, 1997.

[3] S. D. Pendleton, H. Andersen, X. Du, X. Shen, M. Meghjani, Y. H. Eng, D. Rus, and M. H. Ang, "Perception, planning, control, and coordination for autonomous vehicles," *Machines*, vol. 5, no. 1, p. 6, 2017.

[4] (accessed April 17, 2018) Autopilot | Tesla Nederland. https://www.tesla.com/nl_NL/autopilot?redirect=no.

[5] (accessed April 17, 2018) On the Road - Waymo. https://waymo.com/ontheroad/.

[6] M. Kyriakidis, R. Happee, and J. C. de Winter, "Public opinion on automated driving: Results of an international questionnaire among 5000 respondents," *Transportation research part F: traffic psychology and behaviour*, vol. 32, pp. 127–140, 2015.

[7] H. Bellem, B. Thiel, M. Schrauf, and J. F. Krems, "Comfort in automated driving: An analysis of preferences for different automated driving styles and their dependence on personality traits," *Transportation research part F: traffic psychology and behaviour*, vol. 55, pp. 90–100, 2018.

[8] M. Dikmen and C. M. Burns, "Autonomous driving in the real world: Experiences with tesla autopilot and summon," in *Proceedings of the 8th International Conference on Automotive User Interfaces and Interactive Vehicular Applications*. ACM, 2016, pp. 225–228.

[9] S. Scherer, A. Dettmann, F. Hartwich, T. Pech, A. C. Bullinger, and G. Wanielik, "How the driver wants to be driven-modelling driving styles in highly automated driving," in *7. Tagung Fahrerassistenzsysteme*, 2015.

[10] N. M. Yusof, J. Karjanto, J. Terken, F. Delbressine, M. Z. Hassan, and M. Rauterberg, "The exploration of autonomous vehicle driving styles: preferred longitudinal, lateral, and vertical accelerations," in *Proceedings of the 8th International Conference on Automotive User Interfaces and Interactive Vehicular Applications*. ACM, 2016, pp. 245–252.

[11] J. Villagra, V. Milanés, J. Pérez, and J. Godoy, "Smooth path and speed planning for an automated public transport vehicle," *Robotics and Autonomous Systems*, vol. 60, no. 2, pp. 252–265, 2012.

[12] R. Solea and U. Nunes, "Trajectory planning with velocity planner for fully-automated passenger vehicles," in *Intelligent Transportation Systems Conference, 2006. ITSC'06. IEEE*. IEEE, 2006, pp. 474–480.

[13] L. L. Hoberock, "A survey of longitudinal acceleration comfort studies in ground transportation vehicles," *Journal of Dynamic Systems, Measurement, and Control*, vol. 99, no. 2, pp. 76–84, 1977.

[14] L. Svensson and J. Eriksson, "Tuning for ride quality in autonomous vehicle: Application to linear quadratic path planning algorithm," 2015.

[15] T. Hessburg and M. Tomizuka, "Fuzzy logic control for lateral vehicle guidance," *IEEE control systems*, vol. 14, no. 4, pp. 55–63, 1994.

[16] B. Li and F. Yu, "Design of a vehicle lateral stability control system via a fuzzy logic control approach," *Proceedings of the Institution of Mechanical Engineers, Part D: Journal of Automobile Engineering*, vol. 224, no. 3, pp. 313–326, 2010.

[17] T. Hiraoka, O. Nishihara, and H. Kumamoto, "Model-following sliding mode control for active four-wheel steering vehicle," *Review of Automotive Engineering*, vol. 25, no. 3, p. 305, 2004.

[18] A. Norouzi, R. Kazemi, and S. Azadi, "Vehicle lateral control in the presence of uncertainty for lane change maneuver using adaptive sliding mode control with fuzzy boundary layer," *Proceedings of the Institution of Mechanical Engineers, Part I: Journal of Systems and Control Engineering*, vol. 232, no. 1, pp. 12–28, 2018.

[19] F. Yakub, A. Abu, S. Sarip, and Y. Mori, "Study of model predictive control for path-following autonomous ground vehicle control under crosswind effect," *Journal of Control Science and Engineering*, vol. 2016, 2016.

[20] T. Keviczky, P. Falcone, F. Borrelli, J. Asgari, and D. Hrovat, "Predictive control approach to autonomous vehicle steering," in *Proc. of the American Control Conference, 2006*. IEEE, 2006, pp. 6–pp.

[21] T. Besselmann and M. Morari, "Hybrid parameter-varying model predictive control for autonomous vehicle steering," *European Journal of Control*, vol. 14, no. 5, pp. 418–431, 2008.

[22] E. Alcala, V. Puig, J. Quevedo, T. Escobet, and R. Comasolivas, "Autonomous vehicle control using a kinematic lyapunov-based technique with lqr-lmi tuning," *Control Engineering Practice*, vol. 73, pp. 1–12, 2018.

[23] G. Tagne, R. Talj, and A. Charara, "Design and validation of a robust immersion and invariance controller for the lateral dynamics of intelligent vehicles," *Control Engineering Practice*, vol. 40, pp. 81–92, 2015.

[24] J. Kosecka, R. Blasi, C. Taylor, and J. Malik, "Vision-based lateral control of vehicles," in *IEEE Conference on Intelligent Transportation System, 1997. ITSC'97.* IEEE, 1997, pp. 900–905.

[25] P. Belvén, "Implementation of model predictivecontrol for path following with the kth research concept vehicle," 2015.

[26] P. F. Lima, M. Trincavelli, J. Mårtensson, and B. Wahlberg, "Clothoid-based model predictive control for autonomous driving," in *2015 European Control Conference (ECC)*. IEEE, 2015, pp. 2983–2990.

[27] S. Whitsitt and J. Sprinkle, "A passenger comfort controller for an autonomous ground vehicle," in *2012 IEEE 51st Annual Conference on Decision and Control (CDC)*. IEEE, 2012, pp. 3380–3385.

[28] H. Peng and M. Tomizuka, "Vehicle lateral control for highway automation," in *American Control Conference, 1990.* IEEE, 1990, pp. 788–794.

[29] H. Yun, H. Chang, H. Shim, and J. H. Seo, "A preliminary result on frequency-shaped model predictive control," in *2015 IEEE 54th Annual Conference on Decision and Control (CDC)*. IEEE, 2015, pp. 2395–2399.

[30] R. Gondhalekar, C. N. Jones, T. Besselmann, J.-H. Hours, and M. Mercangöz, "Constrained spectrum control using mpc," in *2011 50th IEEE Conference on Decision and Control and European Control Conference (CDC-ECC)*. IEEE, 2011, pp. 1219–1226.

[31] P. Branton, "Ergonomic research contributions to design of the passenger environment," *Person-Centred Ergonomics: A Brantonian View Of Human Factors*, p. 111, 2003.

[32] H. Suzuki, "Research trends on riding comfort evaluation in japan," *Proceedings of the Institution of Mechanical Engineers, Part F: Journal of Rail and Rapid Transit*, vol. 212, no. 1, pp. 61–72, 1998.

[33] W. J. Cheng, "Study on the evaluation method of highway alignment comfortableness," 2007.

[34] J. Xu, K. Yang, Y. Shao, and G. Lu, "An experimental study on lateral acceleration of cars in different environments in sichuan, southwest china," *Discrete Dynamics in nature and Society*, vol. 2015, 2015.

[35] Y. Yamagishi, H. Inooka, and F. Wang, "A study of ride comfort during the turning of a car," *The Japanese Journal of Ergonomics*, vol. 39, no. 4, pp. 162–168, 2003.

[36] A. S. Kilinç and T. Baybura, "Determination of minimum horizontal curve radius used in the design of transportation structures, depending on the limit value of comfort criterion lateral jerk," *TS06G-Engineering Surveying, Machine Control and Guidance, Rome, Italy*, 2012.

[37] C. Gianna, S. Heimbrand, and M. Gresty, "Thresholds for detection of motion direction during passive lateral whole-body acceleration in normal subjects and patients with bilateral loss of labyrinthine function," *Brain research bulletin*, vol. 40, no. 5-6, pp. 443–447, 1996.

[38] Q. Huang and H. Wang, "Fundamental study of jerk: evaluation of shift quality and ride comfort," SAE Technical Paper, Tech. Rep., 2004.

[39] D. Martin and D. Litwhiler, "An investigation of acceleration and jerk profiles of public transportation vehicles," in *Conference Proceedings of ASEE Annual Conference and Exposition*, 2008.

[40] K. Hayafune and H. Yoshida, "Control method of autonomous vehicle considering compatibility of riding comfort and vehicle controllability," SAE Technical Paper, Tech. Rep., 1990.

[41] B. Rao and B. Jones, "An equal sensation study of seated subjects in three translational modes," *Ergonomics*, vol. 21, no. 2, pp. 123–134, 1978.

[42] G. F. Beard and M. J. Griffin, "Discomfort during lateral acceleration: Influence of seat cushion and backrest," *Applied ergonomics*, vol. 44, no. 4, pp. 588–594, 2013.

[43] I. H. Wyllie and M. Griffin, "Discomfort from sinusoidal oscillation in the roll and lateral axes at frequencies between 0.2 and 1.6 Hz," *The Journal of the Acoustical Society of America*, vol. 121, no. 5, pp. 2644–2654, 2007.

[44] C. Corbridge and M. Griffin, "Vibration and comfort: vertical and lateral motion in the range 0.5 to 5.0 Hz," *Ergonomics*, vol. 29, no. 2, pp. 249–272, 1986.

[45] M. J. Griffin and K. L. Mills, "Effect of frequency and direction of horizontal oscillation on motion sickness." *Aviation, space, and environmental medicine*, vol. 73, no. 6, pp. 537–543, 2002.

[46] ——, "Effect of magnitude and direction of horizontal oscillation on motion sickness." *Aviation, space, and environmental medicine*, vol. 73, no. 7, pp. 640–646, 2002.

[47] F. Yakub, S. Lee, and Y. Mori, "Comparative study of mpc and lqc with disturbance rejection control for heavy vehicle rollover prevention in an inclement environment," *Journal of Mechanical Science and Technology*, vol. 30, no. 8, pp. 3835–3845, 2016.

[48] J. Fuller, M. Best, N. Garret, and M. Passmore, "The importance of unsteady aerodynamics to road vehicle dynamics," *Journal of Wind Engineering and Industrial Aerodynamics*, vol. 117, pp. 1–10, 2013.

[49] Y. William, W. Oraby, and S. Metwally, "Analysis of vehicle lateral dynamics due to variable wind gusts," *SAE International Journal of Commercial Vehicles*, vol. 7, no. 2014-01-2449, pp. 666–674, 2014.

[50] M. Abe, *Vehicle handling dynamics: theory and application*. Butterworth-Heinemann, 2015.

[51] E. Thilén, "Robust model predictive control for autonomous driving," 2017.

[52] F. Borrelli, P. Falcone, T. Keviczky, J. Asgari, and D. Hrovat, "Mpc-based approach to active steering for autonomous vehicle systems," *International Journal of Vehicle Autonomous Systems*, vol. 3, no. 2-4, pp. 265–291, 2005.